Phys. Status Solidi A **213,** No. 12, 3078–3102 (2016) / **DOI** 10.1002/pssa.201600281

physica status solidi a
www.pss-a.com
applications and materials science

Feature Article

On the internal quantum efficiency for InGaN/GaN light-emitting diodes grown on insulating substrates

Zi-Hui Zhang[*,1], Yonghui Zhang[1], Wengang Bi[,1], Hilmi Volkan Demir[***,2], and Xiao Wei Sun[****,2,3]**

[1] Key Laboratory of Electronic Materials and Devices of Tianjin, School of Electronics and Information Engineering, Hebei University of Technology, 5340 Xiping Road, Beichen District, Tianjin 300401, P.R. China
[2] LUMINOUS Centre of Excellence for Semiconductor Lighting and Displays, School of Electrical and Electronic Engineering, Nanyang Technological University, 50 Nanyang Avenue, Singapore 639798, Singapore
[3] Department of Electrical and Electronic Engineering, College of Engineering, South University of Science and Technology, 1088 Xue-Yuan Road, Shenzhen, Guangdong 510855, P.R. China

Received 25 April 2016, revised 29 May 2016, accepted 3 June 2016
Published online 28 June 2016

Keywords III-nitride semiconductors, efficiency droop, internal quantum efficiency, light-emitting diodes

[*] Corresponding author: e-mail zh.zhang@hebut.edu.cn, Phone: +86 022 60435772, Fax: +86 022 60438244
[**] e-mail wbi@hebut.edu.cn, Phone: +86 022 60435782, Fax: +86 022 60438244
[***] e-mail volkan@stanfordalumni.org, Phone: +65 67905395, Fax: +65 67912687
[****] e-mail sunxw@sustc.edu.cn, Phone: +86 755 8801 8558, Fax: +86 755 8801 8558

The internal quantum efficiency (IQE) for InGaN/GaN light-emitting diodes (LEDs) grown on [0001] sapphire substrates is strongly affected by various factors including polarization effect in the InGaN/GaN multiple quantum wells (MQWs), insufficient electron and hole injections, low p-type GaN doping efficiency, carrier loss due to the Auger recombination, and current crowding effect especially for the hole current in the p-GaN region. In this work, the remedies taken by the scientific community to enhance the IQE are reviewed, compared and summarized. Meanwhile, this review also discusses alternative ways including polarization self-screening effect, polarization cooling, hole accelerator, and hole modulator. The structural solutions we propose in this work can better improve the device performance without increasing the processing difficulty significantly, and their effectiveness in improving the IQE is further supported by the numerical and experimental studies. For example, on the contrary to common belief, the polarizations in the [0001] oriented InGaN/GaN LEDs can be advantageously used to improve the device performance based on our designs.

1 Introduction III–V Nitride light-emitting diodes (LEDs) have popularly penetrated into the market of the visible light communication, lighting, sensing, and display illumination [1, 2]. It is well known that the III–V nitride LED-based white lighting source is able to yield the efficacy even higher than those traditional light sources such as the incandescent light bulbs by more than 15 times, which leads to a yearly reduction of the CO_2 emission by 1900 Mt [1], and this makes significant contribution to relieve the global warming effect. Additionally, compared to the mercury-based fluorescent light tubes, the III–V nitride solid-state lighting source produces no pollutions on our planet. Therefore, the III–V nitride-based solid state lighting has attracted global intense interest and is regarded as the ultimate lighting approach in this century.

The technology of III–V nitride LED has been developed for more than three decades since Maruska et al. pioneered the world-first single-crystalline GaN material [3]. However, the efficiency of the GaN LED at that time was low due to the poor crystal quality and the absence of the GaN layer with the p-type conductivity. It was found that GaN can be of p-type conductivity through Mg doping and further activated by either thermal annealing in the N_2 ambient [4] or low energy electron beam irradiation [5]. Moreover, the adoption of the GaN [6] or the AlN buffer layer [7] enables the excellent crystalline quality for the subsequently grown GaN epilayers. Although main

obstacles which hinder the development of GaN LEDs have been solved, even more work is still needed to continuously improve the efficiency of GaN LEDs.

In this article, we will firstly briefly discuss various issues that strongly influence the LED efficiency by using the well-known ABC model in Section 2. Then we will review the most recently proposed approaches ever adopted to improve the IQE for LEDs in Section 3. Lastly, we make our conclusion and suggest the future outlooks in Section 4. It shall be noted that the III–V nitride LEDs can be epi-grown on various substrates, e.g., sapphire, SiC, Si, GaN, etc. This review article is mainly focused on the LEDs grown on the [0001] sapphire substrate due to the fruitful and dominant achievements in the past few years.

2 Issues which affect the internal quantum efficiency The architectural energy band for an InGaN/GaN LED is sketched in Fig. 1. Several events take place during the carrier transport which can be linked to the well-known ABC model [8, 9]. The ABC model can be formulated in Eq. (1),

$$\eta_{\mathrm{IQE}} = \frac{\eta_{\mathrm{inj}} \cdot Bn^2}{An + Bn^2 + Cn^3} \tag{1}$$

in which, η_{IQE}, η_{inj}, A, B, C, and n represent the internal quantum efficiency (IQE), carrier injection efficiency, defect-induced Shockley–Read–Hall (SRH) recombination coefficient, bimolecular radiative recombination coefficient, Auger recombination coefficient, and carrier density, respectively. The carrier injection efficiency (η_{inj}) includes the electron injection efficiency and the hole injection efficiency, respectively.

According to Fig. 1, the electrons are supplied by the n-GaN layer while the holes are injected from the p-GaN layer. It is well known that electrons and holes are not synchronized in the transport due to the fact that electrons are more mobile than holes, and the low doping efficiency for the p-GaN layer also strongly reduces the hole injection efficiency and this in turn further results in the electron leakage into the p-GaN layer [10]. Considering the variety on the reported approaches for improving the carrier injection, detailed discussions will be conducted in Sections 3.1 and 3.2.

Mendez et al. have reported the impact of the electric field in separating the electron and hole wave functions and reducing the radiative recombination rate for the GaAs quantum well [11], and this is also well known as the quantum-confined Stark effect (QCSE) for the strained InGaN/GaN [0001] oriented quantum wells, which have very strong spontaneous and piezoelectric polarization-induced electric field [12, 13]. Therefore, one of the key approaches to increase the radiative recombination rate is to screen the polarization effect in the quantum wells [12, 14, 15] and the detailed discussions will be made in Subsection 3.3.

Additionally, the radiative recombination rate is also affected by the current crowding effect [16, 17], which significantly makes the current more unhomogeneously distributed in the quantum well planes, e.g., the current may substantially crowd under the p-electrode. Meanwhile, a high local current density also results in the serious Joule self-heating effect and the increased thermal resistance [18]. It is reported that the current crowding effect increases the ideality factor for the LED device [19], whereas a lager ideality factor is the signature of the non-radiative recombination. Therefore, the proposals to suppress the current crowding will be addressed in Section 3.4.

The IQE is also affected by the defect-related recombination process, denoted as the An [8, 20, 21]. Until now, there is no consensus if the defect-related recombination is responsible for the efficiency droop, which is defined as the decrease of the quantum efficiency for a LED device

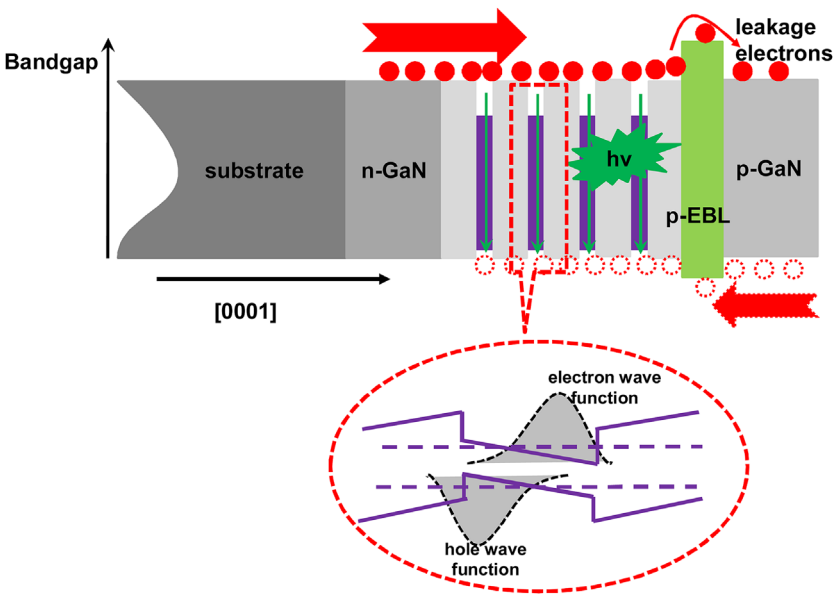

Figure 1 Schematic energy band diagram for the InGaN/GaN LED architecture. Here, p-EBL denotes the p-type electron blocking layer.

as the injection current increases. The report by Schubert et al. shows that the defect-related recombination has a strong impact on the maximum quantum efficiency but does not lead to the efficiency droop [22]. The LED device with a low dislocation density has a pronounced efficiency peak while showing a fast decrease of the quantum efficiency as the injection current further increases. However, the LED device with a high dislocation density exhibits a low peak efficiency accompanied by a small efficiency decrease with the ascending injection current, and in the meanwhile, Shao et al. report that the current where the peak efficiency takes place is also shifted to a higher value once the dislocation density is increased [23]. Nevertheless, the defect-related recombination may contribute to the efficiency droop if the SRH recombination coefficient scales up with the injection current, and this is well modeled by the density-activated defect recombination (DADR) model [24, 25], which takes place when the carrier concentration is high enough to facilitate the carrier delocalization. The DADR model well interprets that the InGaN/GaN quantum well with more InN composition processes a more severe efficiency droop. The methods to suppress the defect-related recombination will be discussed in Section 3.5.

The carriers are also consumed non-radiatively in the quantum wells by the Auger recombination [8, 26]. Different characterization methods and models are used to extract the Auger recombination coefficient [26–33]. For example, through combining the ABC model and the photoluminescence (PL) measurement, Shen and co-workers report that the Auger recombination coefficient ranges from 1.4×10^{-30} to $2.0 \times 10^{-30}\,\mathrm{cm^6\,s^{-1}}$ for thick $In_xGa_{1-x}N$/GaN ($x \sim 9$–15%) double heterostructure (DH) [26]. A room-temperature Auger recombination coefficient of $1.8 \pm 0.2 \times 10^{-31}\,\mathrm{cm^6\,s^{-1}}$ in the bandgap range of 2.5−3.1 eV is contributed by Brendel et al. [27], who extract the Auger recombination coefficient through measuring the optical gain spectra for a GaInN/GaN quantum well laser structure. The Auger recombination coefficient can also be extracted by using the modulation bandwidth studies, which is conducted by Green and co-workers [29]. According to their report, the Auger recombination coefficient is measured to be $1.0(\pm 0.3) \times 10^{-29}\,\mathrm{cm^6\,s^{-1}}$ for the 450 nm InGaN/GaN LEDs. Note, because of the complexity, the density-dependent Auger recombination coefficient has not been taken into consideration in Refs. [26, 27, 29]. The variations for the reported Auger recombination coefficient values may arise from the different methods to extract the Auger recombination coefficient when using the ABC model [26, 27, 29]. A collection of the Auger recombination coefficient for various LED structures have been summarized by Cho et al. [34] and Piprek et al. [8, 35]. It is worth mentioning that, according to the report by Piprek, the Auger recombination coefficient that is smaller than $10^{-30}\,\mathrm{cm^6\,s^{-1}}$ seems less likely to cause the efficiency droop [8]. However, despite the disputations [36, 37], it has reached a consensus that the Auger recombination is among the sources causing the efficiency droop and has to be reduced. The methods employed by different groups to suppress the Auger recombination will be then summarized in Section 3.6.

In view of the above discussions, those limiting factors that hinder the IQE for InGaN/GaN LEDs have to be overcome by the III–V nitride community. This article will mainly review the approaches and also propose the design principles for different InGaN/GaN LED structures to enhance the LED performance and reduce the efficiency droop.

3 Approaches for improving the internal quantum efficiency

3.1 Design strategies to increase the electron efficiency for nitride light-emitting diodes One factor which matters the InGaN/GaN LED IQE is the electron injection [8, 34, 38]. In order to increase the electron injection efficiency, there have been many effective designs proposed by the III-nitride community. Here, we will review and list some of those typical methods employed. To enhance the electron injection (i) one can engineer the p-EBL so that the electrons have less chance of escaping from the active region; (ii) one can also increase the electron capture rate by designing novel quantum well/quantum barrier structures; (iii) the electron energy can be decreased before being injected into the active region so that the quantum wells are able to more efficiently trap the electrons and prevent them from directly overflying into the p-GaN region; and (iv) an increased hole injection efficiency is very useful in making better use of the electrons for radiative recombination. Nevertheless, the hole injection efficiency will be discussed in Section 3.2.

3.1.1 Increase of the electron blocking effect for the p-EBL Whenever discussing the electron leakage reduction, it comes into the mind that the p-EBL has to be engineered. Therefore, tremendous efforts have been paid to improve the p-EBL. Currently, for the [0001] oriented LEDs, the p-AlGaN is mostly used as the EBL, which is lattice-mismatched to the GaN quantum barrier and causes the strong polarization effect, while the polarization effect leads to the electron accumulation and reduces the effective conduction band barrier height, which in turn facilitates the electron leakage [39]. The polarization inverted p-EBL (i.e., [000-1] orientation) can eliminate the electron accumulation [40]. However, this structure induces the post-bonding difficulties thus making it less reliable in reality. Some groups suggest inserting a p-InGaN before growing the p-AlGaN EBL to reduce the electron leakage [41–45], but the origin on the reduced electron leakage is unclear till now. This can nevertheless be well explained by the polarization inversion effect. As has been mentioned, for the [0001] oriented GaN/p-AlGaN structure, there is very strong polarization appearing at the interface and giving rise to the polarization interface charges of positive polarity, which significantly bends the conduction band of the GaN quantum barrier downwards. However, if the GaN quantum barrier is replaced by GaN/$In_xGa_{1-x}N$ heterojunction, then the

interface between GaN layer and $In_xGa_{1-x}N$ layer is polarized by yielding negative charges, and the conduction band of the GaN layer will be bent in the way favoring the electron blocking. Such different band bending details have been well calculated and can be found in Ref. [44], and they are now presented in Fig. 2(a) and (b). Clearly, we can see that the GaN last quantum barrier in Fig. 2(a) favors the electron accumulation at the interface of GaN/p-AlGaN, and this further leads to the electron leakage into the p-GaN side. However, the GaN/$In_xGa_{1-x}N$ architecture possesses the negative polarization-induced charges, and these charges upwards bend the conduction band as shown in Fig. 2(b), and this increases the blocking effect of the last quantum barrier, thus suppressing the electron leakage and improving the LED efficiency. The effective conduction band barrier heights are shown in Table 1.

Kim et al. propose the lattice-matched InAlN p-EBL so that the GaN/InAlN heterojunction is free from any piezo-polarization effect, and this helps to better confine the electrons and then improve the quantum efficiency in the green regime [46]. InAlN as the p-EBL also proves to be effective in reducing the electron spill-over level in the blue InGaN/GaN LEDs by Choi et al. [47, 48]. Despite the success of growing the InAlN material, to achieve the epitaxial InAlN compound is still more challenging than to grow the AlGaN layer. Recently, we suppress the polarization discontinuity by using the polarization self-screening effect, and it is proved to be effective in reducing the polarization-induced electric field in the [0001]-oriented quantum wells [49] (the details of the polarization self-screening effect will be demonstrated in Section 3.3). Then, we apply the polarization self-screening effect to the p-EBL for reducing the polarization discontinuity

Table 1 The effective conduction band barrier heights for the studied device at 20 A cm^{-2} in Ref. [44].

device	$\Delta\Phi_{e\text{-LQB}}$ (meV)	$\Delta\Phi_{e\text{-EBL}}$ (meV)	$\Delta\Phi_{h\text{-EBL}}$ (meV)
reference device	210	325	469
three-step graded u-InGaN LQB device	362	490	358

Reproduced from Ref. [44], with the permission of AIP publishing.

and the electron leakage [50]. Compared to those InAlN and InAlGaN p-EBLs, the polarization self-screened p-EBL can easily be grown by using the MOCVD technology. The schematic layer diagrams of the p-EBL for the studied devices are shown in Fig. 3(a) and (b), respectively. Figure 3(a) illustrates the InGaN/GaN LED with a conventional AlGaN p-EBL. Investigation into Fig. 3(a) shows the positive polarization-induced interface charges at the GaN/AlGaN interface, which strongly cause the electron accumulation and bend the conduction band of the GaN region. According to Ref. [51], we obtain the formula of $\Phi_b = \Delta E_C - kT \cdot \ln(n_{LB/EBL}/N_C)$, and it shows that the effective conduction band barrier height (Φ_B) is co-affected by ΔE_c, T, $n_{LB/EBL}$, and N_c which denote the conduction band offset between the GaN last barrier (LB) and the p-EBL, the carrier temperature, the electron concentration at the LB/EBL interface, and the density of states for electrons, respectively. Therefore, one way to increase Φ_B is to decrease $n_{LB/EBL}$, and this can be achieved by the p-EBL architecture presented in Fig. 3(b). The p-EBL in Fig. 3(b) is grown by the metal-organic chemical vapor deposition (MOCVD) system in the way that

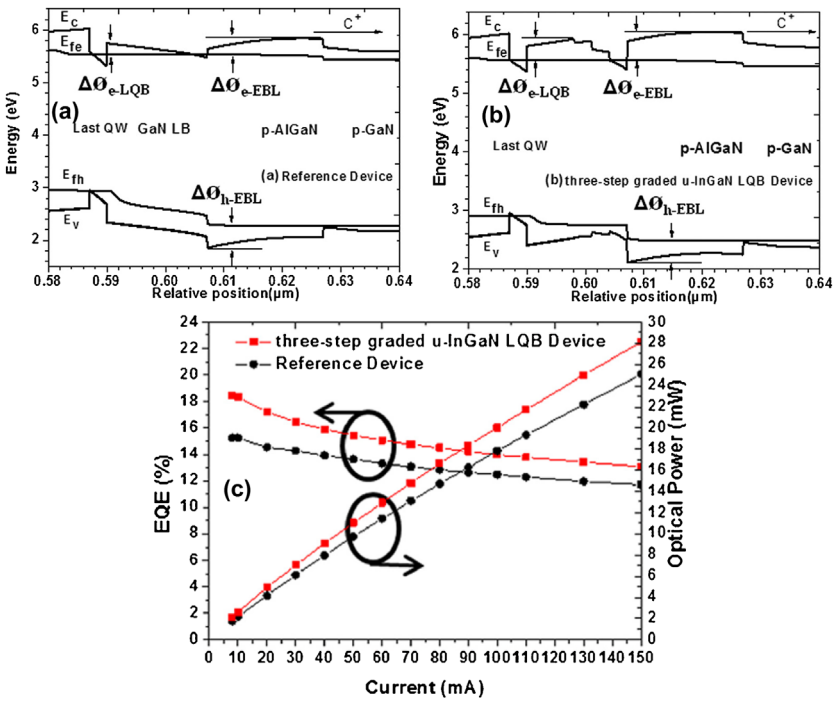

Figure 2 Energy band alignments in the vicinity of (a) the GaN last quantum barrier (LB) and p-AlGaN EBL and (b) the GaN/$In_xGa_{1-x}N$/p-AlGaN EBL, for the two InGaN/GaN LEDs, respectively. Here, Fig. 2(b) uses the three-step graded InGaN LQB (last quantum barrier) architecture, with a 3 nm-$In_{0.015}Ga_{0.985}N$/3 nm-$In_{0.052}Ga_{0.948}N$/3 nm-$In_{0.09}Ga_{0.91}N$ structure. Data are collected at 20 A cm^{-2}. (c) Experimentally measured EQE and the optical power for the two LEDs. Reproduced from Ref. [44], with the permission of AIP publishing.

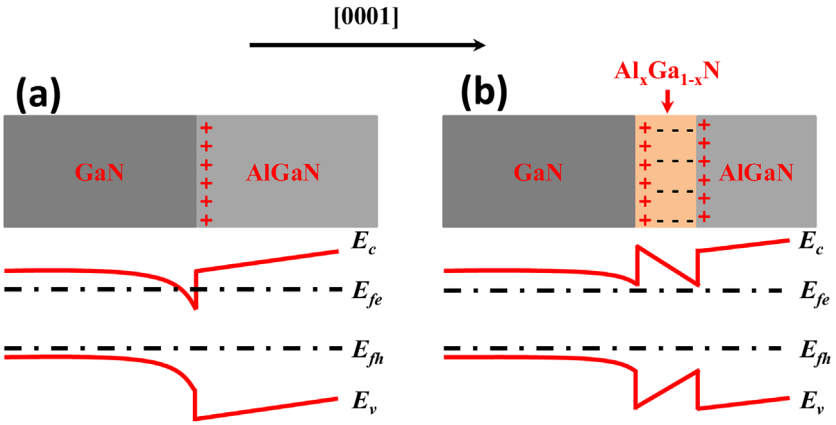

Figure 3 Schematic energy band diagrams of (a) conventional GaN/p-EBL architecture, in which the p-$Al_{0.20}Ga_{0.80}N$ EBL is 20 nm thick and (b) proposed polarization self-screened GaN/p-EBL architecture for InGaN/GaN LEDs, in which the AlN composition follows a linear grading from 20% to 0.0% in 10 nm thickness and the rest p-$Al_{0.20}Ga_{0.80}N$ EBL is 10 nm. Reproduced from Ref. [50], with the permission of AIP publishing.

the $Al_xGa_{1-x}N$ region has the AlN compositionally graded from 20.0% to 0.0% along the [0001] growth direction within the 10 nm range, and as the result, the negative polarization induced bulk charges (ρ_B^{Pol}) are produced, which can screen the polarization-induced positive interface charges (σ_B^{Pol}). Therefore, the electrons will be less accumulated at the GaN/p-$Al_xGa_{1-x}N$ interface that enables a reduction of $n_{LB/EBL}$ and then increases Φ_B, leading to a better electron confinement. The rest $Al_{0.20}Ga_{0.80}N$ layer is 10 nm thick. We assume a 40% polarization level due to the strain release by generating the dislocations during the epitaxial growth process [52]. The σ_B^{Pol} between the GaN last barrier and the p-$Al_{0.20}Ga_{0.80}N$ EBL is 0.36×10^{17} m^{-2} while the ρ_B^{Pol} in the $Al_xGa_{1-x}N$ region is found to be -3.74×10^{24} m^{-3}. The details for calculating the σ_B^{Pol} and ρ_B^{Pol} can be found in Ref. [50].

We define $\Delta\phi$, Φ_{b1}, and Φ_{b2} as bending level of the last quantum barrier, effective conduction band barrier height between the last quantum barrier and the p-EBL, and the effective conduction band barrier height of the rest p-EBL region, respectively. Φ_{b3} denotes the effective valence band barrier height between the last quantum barrier and the p-EBL, while Φ_{b4} presents the effective valence band barrier height of the rest p-EBL region. Investigation of Fig. 4(a) and (b) demonstrates that $\Delta\phi$ is smaller in the polarization self-screened p-EBL architecture, which means the last quantum barrier is more effective in confining the electrons. Meanwhile the values of Φ_{b1} and Φ_{b2} in Fig. 4(b) are larger than those in Fig. 4(a), and this represents a reduced electron leakage level for the p-EBL. On the other hand, the two devices have the identical Φ_{b3} and Φ_{b4}, which translate to the unaffected hole injection by the polarization self-screened p-EBL structure. Hence, both the quantum efficiency and the efficiency droop for the LED device with the polarization self-screened p-EBL has been improved

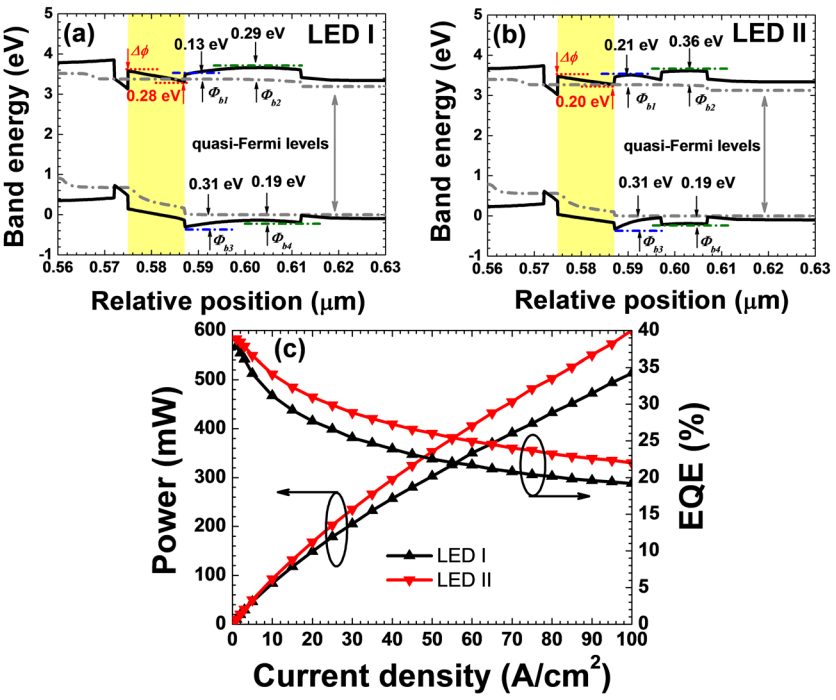

Figure 4 Numerically calculated energy band diagrams in the vicinity of the p-EBL and the values of $\Delta\phi$, Φ_{b1}, Φ_{b2}, Φ_{b3}, and Φ_{b4} for (a) the LED device with bulk-type p-AlGaN EBL at 30 A cm^{-2}, (b) the LED device with the polarization self-screened p-EBL at 30 A cm^{-2}. (c) Experimentally measured EQE and the optical power for the two LEDs. Reproduced from Ref. [50], with the permission of AIP publishing.

according to Fig. 4(c), such that the quantum efficiency for LED II is enhanced by 16.9% at 100 A cm^{-2} when compared to LED I, and the efficiency droop at 100 A cm^{-2} for LED I and II is 49.3% and 42.3%, respectively.

Recently, chirped multiple-quantum-barrier (MQB) type p-EBL is proposed and proves to be useful in reducing the electron leakage and improv-ing the internal quantum efficiency for the InGaN/GaN LEDs [53–55]. By properly tuning superlattice-type MQB thickness, the MQB structure creates the forbidden energy bands above the natural conduction band edge, and this cuts off the resonant tunneling for electrons, hence facilitating the electron reflectivity and reducing the electron leakage rate. However, according to the report by Piprek et al. [56], the origin of the improved quantum efficiency by the chirped MQB type p-EBL is attributed to the enhanced hole injection. The enhanced hole injection efficiency arises from the strong hole accumulation at the AlGaN/p-GaN interface, which are caused by the negative polarization-induced charges. Piprek et al. believe that the electrons leakage is also the consequence of the poor hole injection. The same conclusion is also made by us [57]. However, discussions on the hole injection will be conducted subsequently.

3.1.2 Increase of the electron blocking effect for active region Another approach for increasing the electron injection efficiency is to modify the quantum wells and quantum barriers so that the conduction band offset can be increased and the electron thermionic escape can be suppressed. Currently, GaN is used as the quantum barrier material, and the electron injection can be enhanced if AlGaN with an optimized AlN composition is employed. The numerically simulated results by Chang et al. demonstrate the advantage of AlGaN barriers in improving the electron confinement [58]. Zhao et al. report that a high electron current injection efficiency can be realized by using thin large bandgap barrier (1–2.5 nm), such that a thin AlGaN layer is embedded between the InGaN quantum well and the GaN quantum barrier [59, 60]. Besides, Liu et al. suggest that a high electron injection efficiency can also be obtained by inserting a thin (1–2 nm) InAlGaN or InAlN cap layer such as GaN/InAlGaN/InGaN/InAlGaN/GaN and GaN/InAlN/InGaN/InAlN/GaN structures, respectively [61]. The polarization-matched AlGaInN barriers are also advisable for achieving a high electron confinement [62, 63]. Kuo et al. demonstrate that the GaN/InGaN/GaN-type quantum barriers enable electrons to be injected more efficiently into the quantum wells, giving rise to a reduced efficiency droop and a high quantum efficiency [64]. Later on, Kuo et al. report that the InGaN/AlGaN/InGaN quantum barrier can also increase the electron injection efficiency and achieve a reduced efficiency droop [65]. However, the mechanism on how the GaN/InGaN/GaN- and InGaN/AlGaN/InGaN-type quantum barriers are better in manipulating the electron injection than the conventional GaN quantum barriers are not provided in their works. Besides increasing the conduction band offset through the alloy engineering, by properly increasing the thickness of the last quantum barrier, the electron leakage current can also decrease [66]. Their numerically simulated results are shown in Fig. 5(a) with the 8 nm thick undoped last quantum barrier;

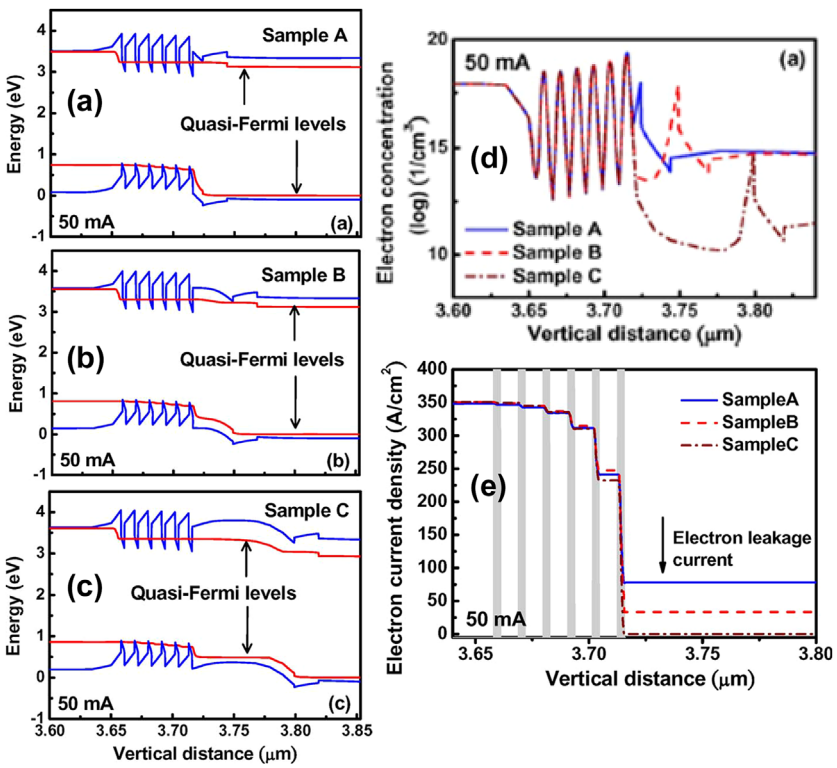

Figure 5 Energy band diagrams for (a) sample A with 8 nm thick undoped last quantum barrier, (b) sample B with 25 nm thick partially p-doped (8 nm undoped +17 nm p-doped) last quantum barrier, (c) sample C with 75 nm thick partially p-doped (8 nm undoped +67 nm p-doped) last quantum barrier. (d) Electron concentration profiles, and (e) electron current leakage levels at 50 mA. The device mesa size is $250 \times 580\ \mu m^2$. Reproduced from Ref. [66], with the permission of Institute of Electrical and Electronics Engineers.

Fig. 5(b) with the 25 nm thick partially p-doped (8 nm undoped +17 nm p-doped) last quantum barrier; Fig. 5(c) with the 75 nm thick partially p-doped (8 nm undoped +67 nm p-doped) last quantum barrier; and Fig. 5(d) and (e), in which we can see that when the last quantum barrier increases the length, the electron accumulation at the last quantum barrier/p-EBL interface is reduced, as shown in Fig. 5(d), while a reduced electron accumulation helps to suppress the electron leakage [50]. As the details for the carrier transport models are not provided in their article, we believe a thicker last quantum barrier reduces the electron intraband tunneling process, and this in turn further alleviates the electron accumulation level at the last quantum barrier/p-EBL interface. For that reason, Fig. 5(e) shows that the electron leakage current level has been substantially decreased thanks to the thicker last quantum barrier. Besides, to avoid the hole blocking effect, they purposely adopt the partially p-doped last quantum barrier when the quantum barrier is thickened.

3.1.3 "Cool down" electrons The other alternative method to enhance the electron injection is to make electrons "cold." This can only be realized by manipulating the electron energy before they enter the quantum well region, and more importantly, this design will not affect the hole injection. The layer which can make electrons "cold" is named as the electron cooler, electron injector, or electron reservoir layer. Otsuji et al. publish their results addressing the effect of the InGaN electron reservoir layer on the electroluminescence efficiency for InGaN/GaN LEDs [67], and they attribute the improved device performance to the enhanced electron capture efficiency by the quantum wells. They tentatively ascribe the increased electron capture efficiency to the variation of the potential field distribution in the quantum wells. Later on, Li et al. conclude that the InGaN insertion layer can reduce the internal electric field in the quantum well through observing the wavelength blueshift of the cathodoluminescence (CL) spectra and a reduced carrier lifetime derived from the time-resolved CL spectra [68]. More importantly, Li et al., by the electron holography, also measure and show a reduced electrostatic potential for the LED device with the InGaN insertion layer [68]. However, a most recent physical model has been developed by Ni et al. [69], Zhang et al. [70], Li et al. [71, 72], Avrutin et al. [73], Zhang et al. [74], and Chang et al. [75] that a reduced electron leakage is caused by the phonon-electron scattering taking place in the InGaN insertion layer. During the phonon-scattering process, the

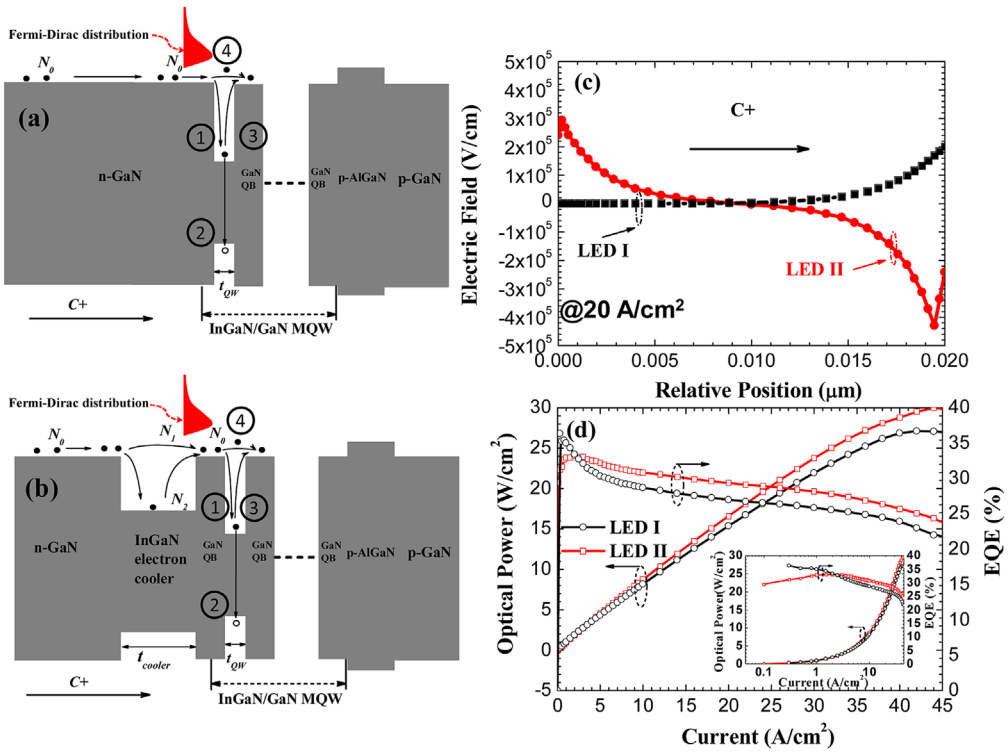

Figure 6 (a) InGaN/GaN LED structure without the EC layer, i.e., LED I, (b) InGaN/GaN LED structure with the EC layer, i.e., LED II. Four electron/transport processes are shown in (a) and (b): ① electrons are captured into the quantum well, ② electrons recombine with holes and at defects, ③ electrons re-escape from the quantum well, and ④ electrons directly fly over to a remote position without being captured by the quantum well. (c) Calculated field profiles in the EC layer for LED II and in the GaN layer for LED I. (d) Experimentally measured EQE and optical power for the two LEDs. Reproduced from Ref. [74], with the permission of Optical Society of America.

electrons lose the energy of 92 meV, such that electrons become "cold" and the InGaN insertion layer functions as the "electron cooler (EC)." In addition, the study by Zhang et al. further reveals the impact of the polarization-induced electric field in the [0001]-oriented InGaN EC layer on the electron energy [74]. The device architectures and the field profiles in the InGaN EC layer are shown in Fig. 6(a)–(c), respectively. The field intensity for LEDs I and II is calculated at 20 A cm^{-2}, and by following $qV = \int_0^{t_{\text{cooler}}} q \times E(y)\text{d}y$, the electrons in LED I lose the kinetic energy of 48.10 meV. The kinetic energy of the electrons in LED II is increased by 27.82 meV due to the polarization-induced electric field in LED III, and therefore, the electrons will lose the energy of 64.18 meV (92–27.82 meV) during the transport in the InGaN EC layer for LED II. As the result, LED II still has more chances of capturing electrons into the quantum wells than LED I, which experimentally translates into a reduced efficiency droop of 18.3% from 24.0% and the quantum efficiency enhancement of 7.8% at 35 A cm^{-2} (Fig. 6(d)). In the meanwhile, the findings by Zhang et al. also indicate that, in order to suppress the acceleration effect by the EC layer to electrons, the thickness and the InN composition in the [0001]-oriented InGaN EC layer have to be well controlled [74].

The effect of the polarization-induced electric field on the electron thermal energy also interprets the origin of the n-AlGaN EBL in reducing the electrons leakage for the [0001]-oriented LEDs, such that in the n-AlGaN EBL, the polarization-induced electric field further reduces the electron thermal energy [76]. The electric fields are calculated at 25 A cm^{-2} and shown in Fig. 7(a). By following $qV = \int_0^{t_{\text{cooler}}} q \times E(y)\text{d}y$, the electrons lose the energy of 62.6 and 105.7 meV for the reference LED sample and the sample with n-EBL, respectively. Thus, electrons will be less mobile after going through the n-EBL, which translates the reduced electron leakage level in Fig. 7(b) and the enhanced optical power in Fig. 7(c). Note, the effectiveness of the n-AlGaN EBL in decreasing the electron leakage level has been previously reported by Yen et al. [77] and Ji et al. [78], however, the origin on the reduced electron leakage by the n-EBL is unclear till now [76].

To summarize, this subsection reviews the methods that have been employed to reduce the electron leakage level and increase the electron injection efficiency in the multiple quantum wells. In order to meet the required targets, the p-EBL has to be engineered either by reducing the lattice mismatch between the p-EBL and the last quantum barrier or by manipulating the polarization charge polarity/

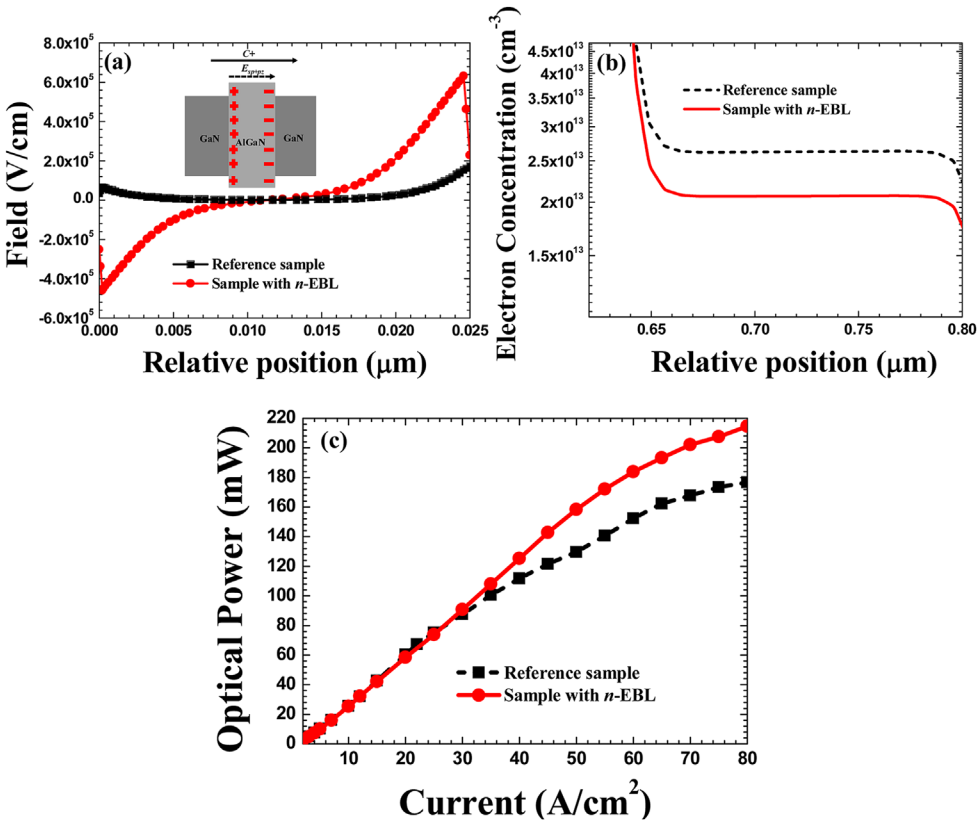

Figure 7 (a) Electric field profiles at 25 A cm^{-2} in the n-GaN layer and n-AlGaN EBL for the reference LED sample and the sample with n-EBL, respectively. Inset figure depicts the polarized n-GaN/n-AlGaN/n-GaN structure. (b) Calculated electron leakage level at 25 A cm^{-2}, and (c) experimentally measured optical power. Reproduced from Ref. [76], with the permission of AIP publishing.

polarization charge density at the interface between the p-EBL and the last quantum barrier. In addition, the quantum barrier height can be properly increased through material engineering, e.g., AlGaN thin cap layer. Lastly, the electron injection mechanism can be tuned before entering the quantum wells, such that we "cool down" electrons and make them less energetic, which can be obtained by using the InGaN electron cooler layer and the n-AlGaN electron blocking layer. More importantly, we also report the impact of the polarization-induced electric field in affecting the electron kinetic energy, therefore, requiring the thickness and the alloy composition for the InGaN electron cooler layer and the n-AlGaN electron blocking layer to be well controlled.

3.2 Design strategies to increase the hole injection efficiency for nitride light-emitting diodes

3.2.1 Reducing the hole blocking effect for the p-EBL The electron leakage is also the consequence of the declining hole injection efficiency. This is easily interpreted by the bimolecular rate equation $R = B \cdot n \cdot p$ that an increased hole concentration (p) in the quantum wells consumes more electrons (n) for achieving more efficient radiative recombination (R), which in turn reduces the electron leakage out of the active region. However, the current InGaN/GaN LED architectures employ the p-type AlGaN electron blocking layer, which also hinders the hole injection due to the valence band offset between the AlGaN and the p-GaN layers [79, 80]. Therefore, a straightforward way to promote the hole injection is to suppress the hole blocking effect by the p-EBL. For that, tremendous efforts have been paid to develop novel p-EBL structures, such as the superlattice p-EBL [81–84]. It has been reported by Schubert et al. that the superlattice p-EBL increases the activation of the deep Mg dopants [85–87]. Meanwhile, the staircase p-EBL is also useful in facilitating the hole injection [88–91]. The staircase p-EBL can then be further modified by linearly grading the AlN composition [92–95], which proves to be effective in further reducing the hole blocking effect by the p-EBL. Recently, some groups report the AlGaN/GaN/AlGaN-type p-EBL to increase the hole injection across the p-EBL [51, 96, 97]. The insertion of the GaN layer helps to reduce the overall valence band barrier height in the p-EBL and more importantly, a wide GaN insertion layer reduces the AlGaN thickness if the total thickness of the p-EBL is a constant, and this in turn triggers the hole intraband tunneling process [96]. Specifically, we further propose the hole injection enhancement through the subband tuning effect, which indicates that the position of the GaN insertion layer is essential in favoring the hole injection [51], as shown in Fig. 8. First of all, the GaN insertion layer has to be very thin (1 nm thick GaN is grown in Ref. [51]) to produce the subbands in the so-called AlGaN/GaN/AlGaN quantum well, and then the thin GaN insertion layer has to be selected at the position close to the p-GaN side, e.g., $x = 3.5$ nm in

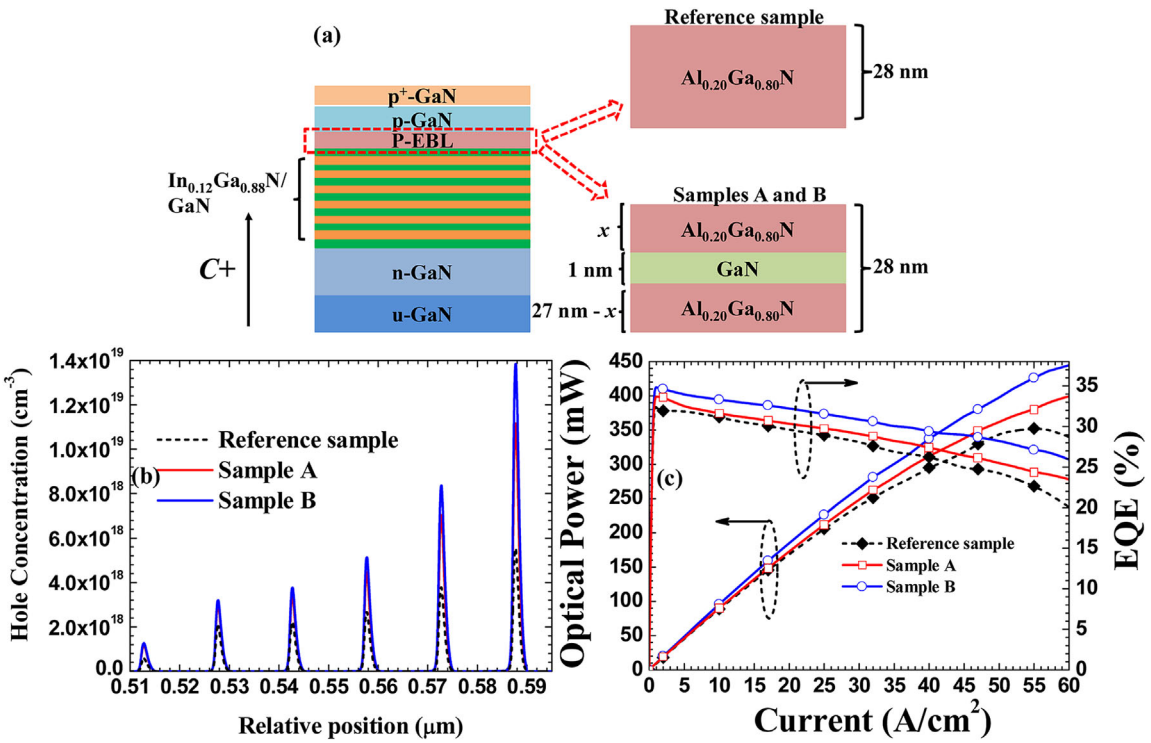

Figure 8 (a) Schematic diagrams for the reference sample and for samples A ($x = 13.5$ nm) and B ($x = 3.5$ nm). (b) Numerically calculated hole concentration in MQW region at 30 A cm^{-2} and (c) experimentally measured optical output power and EQE for the reference sample, samples A and B. Reproduced from Ref. [51], with the permission of Optical Society of America.

Fig. 8(a). By doing so, the remaining 3.5 nm thick AlGaN layer guarantees a smooth hole tunneling into the thin GaN insertion layer and leads to a high hole concentration in the thin GaN layer, denoted as $p_{\text{p–GaN}}$. Besides, the holes occupy the subbands in the thin GaN layer. Originally the valence band barrier height can be formulated by $\Phi_b = \Delta E_V - kT \ln\left(p_{\text{p-GaN}}/N_V\right)$, in which N_V is the effective density of states for holes, k is the Boltzmann constant and ΔE_V is the valence band edge difference between GaN and AlGaN layers, i.e., $\Delta E_V = E_{V\_GaN} - E_{V\_AlGaN}$. Then ΔE_V is replaced by ΔE_{Vi} if holes occupy the subbands in the thin GaN layer. Here $\Delta E_{Vi} = E_{Vi\_GaN} - E_{V\_AlGaN}$, where E_{Vi_GaN} is the quantized subvalence band edge of the thin GaN layer in the p-AlGaN/GaN/p-AlGaN EBL, and it is easily obtained that ΔE_{Vi} is smaller than ΔE_V. It shall also be noted that a high $p_{\text{p–GaN}}$ can further reduce Φ_b. Therefore, employing a thin GaN insertion layer in the p-EBL is useful in promoting the hole injection. More importantly, the position of the thin GaN insertion layer in the p-EBL is crucially important and we recommend that the GaN insertion layer has to be close to the p-GaN side. Figure 8(b) proves that the subband in the thin GaN insertion layer enables a higher hole concentration in the MQW region whereas Fig. 8(c) presents the measured optical output power and the external quantum efficiency for the LED samples. Thanks to the subband tuning effect on the hole injection, both samples A and B show improved optical performance than the reference sample with sample B yielding the strongest intensity.

3.2.2 Increase of the hole injection by producing "hot" holes Besides engineering the p-EBL for increasing the hole injection, we have also proposed and demonstrated a hole accelerator embedded in the p-GaN layer, which promises the effectiveness in increasing the kinetic energy of the holes [98], so that the holes have more chance of climbing over the p-EBL. The schematic energy band diagram for the hole accelerator is shown in Fig. 9(a), in which a thin AlGaN layer (L2) is embedded in the L1 and L3 layers. As the structure is grown along the [0001] orientation, thus the polarization induced electric field is generated in the L3 layer. The magnitude of the polarization-induced electric field is calculated and illustrated in Fig. 9(b), from which we can infer that holes will obtain the additional energy when traveling in the L3 region and the partial L1 region. However, the negative work will be applied to holes in the L2 region. Thus, the net work done to the holes by the polarization-induced electric field can be calculated by following $W = e\int_0^l E_{\text{field}} \cdot dx$. For a comparative study, the integration range starts from the interface of the p-type EBL and the neighboring p-GaN, then ends at the relative position of 0.72 μm as shown in Fig. 9(b), as beyond this range, the electric field for LEDs A and B are identical. Note that LED A does not have the hole accelerator while LED B has the hole accelerator defined in Fig. 9(a). The integration yields the W of 0.087 and 1.069 eV for LEDs A and B at 100 A cm^{-2}, respectively, which translates a higher hole concentration in the quantum wells for LED B than for LED A as presented in Fig. 9(c). We also measure the optical power and the external quantum efficiency for LEDs A and B that is demonstrated in Fig. 9(d). Clearly we can see that the efficiency droop has been reduced from 54.2% to 35.9% at 100 A cm^{-2}.

3.2.3 Increase of the hole injection by improving the hole concentration in the p-GaN layer The hole injection is also affected by the doping efficiency of the p-GaN layer. Currently, the thermal annealing process to activate the Mg dopants in the p-GaN layer is indispensable during the LED epitaxial growth [4]. However, the hole concentration is still not competitive to the electron concentration in the n-GaN layer, which

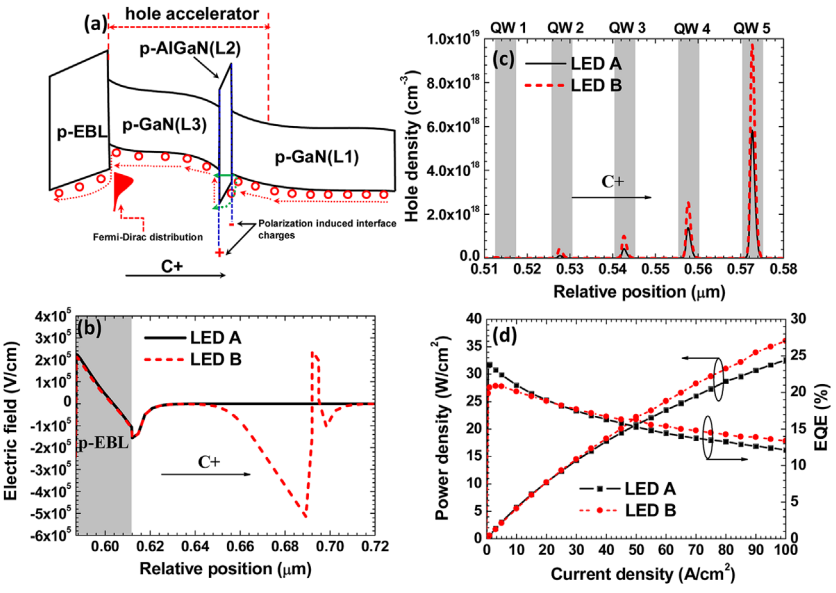

Figure 9 (a) Schematic energy band diagram for the hole accelerator, (b) calculated electric field profiles for LEDs A and B at 100 A cm^{-2}, (c) calculated hole concentration in the quantum wells for LEDs A and B at 100 A cm^{-2}, and (d) experimentally measured optical output power and the external quantum efficiency for LEDs A and B. Reproduced from Ref. [98], with the permission of AIP publishing.

can easily achieve the concentration of $5 \times 10^{18}\,\mathrm{cm}^{-3}$. According to $\Phi_b = \Delta E_V - kT\ln(p_{p-\mathrm{GaN}}/N_V)$ [51], if the hole concentration ($p_{\mathrm{p-GaN}}$) in the p-GaN layer is low, the valence band barrier height (Φ_b) in the p-EBL will be large. Thus, tremendous efforts ought to be paid to improve the hole concentration in the p-GaN layer. Schubert et al. have reported the AlGaN/GaN superlattice doping [85–87], and the Mg activation energy can be further reduced if the Al composition is increased, such that the Mg activation energy is 70 and 58 meV for $Al_{0.10}Ga_{0.90}N$/GaN superlattice and $Al_{0.20}Ga_{0.80}N$/GaN superlattice, respectively, which values are much smaller than the Mg activation energy (170–200 meV) in the p-GaN layer [87]. This idea has been applied to the InGaN/GaN LED architecture which adopts the AlGaN/GaN superlattice as the p-EBL [82, 84].

Besides the superlattice AlGaN/GaN structures, three-dimensional hole gas (3DHG) is also proposed for the N-polar GaN LED by Simon et al. [95], such that the Mg dopants can be more effectively ionized by the polarization-induced electric field in the AlGaN layer if the AlN composition is graded. Meanwhile, unlike the GaN:Mg structure, the resistivity of the 3DHG structure declines when the temperature decreases, and the hole concentration for the 3DHG structure is unchanged even the temperature is at 100 K, which is indicative that there is no carrier free-out for the 3DHG structure even at low temperatures. The electroluminescence (EL) spectra, optical output power for the N-polar GaN devices and the device architectures (i.e., conventional p–n junction LED structure and the polarization-doped p–n junction LED structure, both devices have the mesa areas of $80 \times 150\,\mu\mathrm{m}$) are shown in Fig. 10. Figure 10(a) and (b) shows that the polarization-doped LED processes higher optical intensity than the conventional LED. Figure 10(c) shows the schematic energy band diagrams under the equilibrium for the two LEDs. It shall also be noted that the 3DHG can also be generated in the Ga-polar III-nitride semiconductors [94, 99–102].

In addition to the 3DHG structure, we have also proposed a hole modulator to increase the hole concentration for the p-GaN layer [57], which is demonstrated in Fig. 11. The hole modulator is realized by Mg doping the last quantum barrier. The Mg-doped last quantum barrier has ever been reported by Kuo et al. [103], however, the enhanced hole injection is still unclear until now. As shown in Fig. 11(a), the holes donated by the Mg-doped last quantum barrier are depleted and stored in the p-GaN layer, which can increase the overall hole concentration for the p-GaN layer and facilitates the hole injection when the device is biased (Fig. 11(b)). We also calculate the equilibrium hole distribution for the two LEDs (LED A has no hole modulator and LED B has the hole modulator), as shown in Fig. 11(c). Moreover, by measuring the capacitance–voltage characteristics for LEDs A and B, we obtain the spatial hole profiles (Fig. 11(d)). The experimentally measured hole profiles agree well with the numerically calculated values such that LED B has a higher hole concentration in the p-GaN layer than LED A. Note that the holes of LED B are aligned in the two-dimensional (2D) manner due to the negative polarization-induced interface charges at the p-AlGaN/p-GaN interface. A reduced electron leakage level is simultaneously obtained thanks to the enhanced hole injection efficiency, and for that reason, the external quantum efficiency is increased by 25.59% at $80\,\mathrm{A\,cm}^{-2}$ for the LEDs in the 450 nm regime (Fig. 11(e)).

3.2.4 Increase of the hole injection by improving the hole transport in active region Meanwhile, the insufficient hole injection is also reflected by the non-uniform hole distribution in the multiple quantum wells.

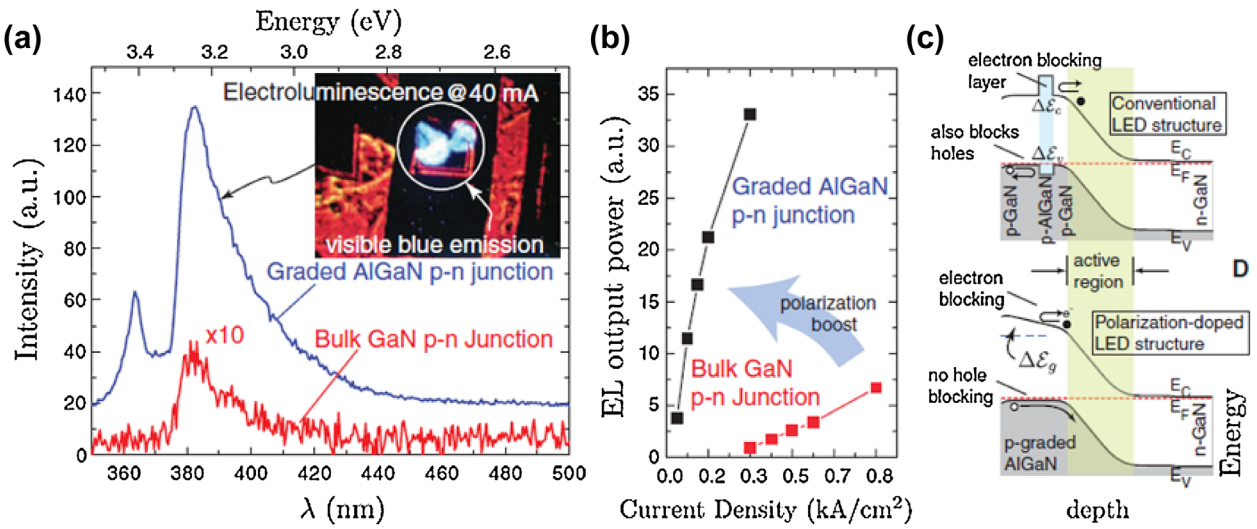

Figure 10 (a) Room temperature EL spectra, the inset figure shows the optical microscope image of the blue emission from the polarization-doped LED structure, (b) relative EL output power, (c) schematic energy band diagrams for the conventional LED structure and the polarization-doped LED structure. Reproduced from Ref. [95], with the permission of AAAS.

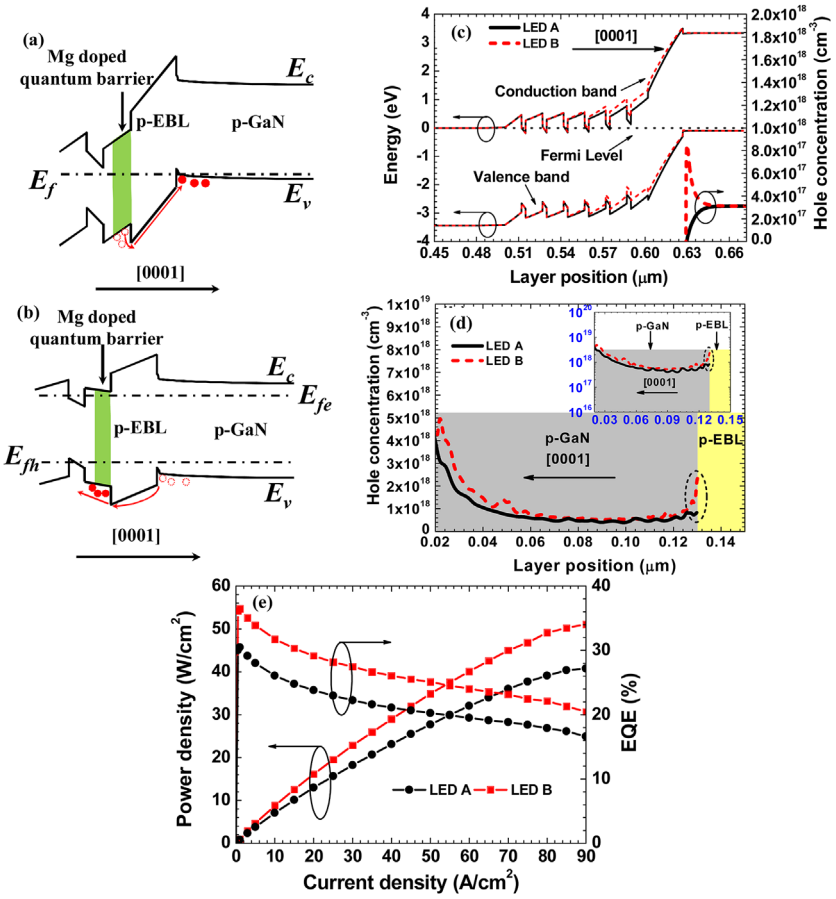

Figure 11 Schematic energy band diagrams for a hole modulator (a) at the equilibrium state, (b) when the device is biased. (c) Calculated energy band diagrams and the hole profiles at the equilibrium state, (d) experimentally measured hole profiles, and (e) experimentally measured EQE and power density for LEDs A and B. Reproduced from Ref. [57], with the permission of AIP publishing.

The holes can be more evenly distributed in the MQW region by replacing the GaN quantum barriers with InGaN quantum barriers [104, 105]. Playing with the quantum well thickness is also helpful to homogenize the hole density in the quantum wells [106, 107], and Wang at al. suggest properly thickening the quantum wells along the [0001] growth orientation [106]. Besides engineering the quantum well thickness, a design of properly thinning the quantum barriers is able to promote the hole injection [108, 109]. Most recently, Piprek has proposed and presented a cascaded active region, which theoretically promises the super hole injection efficiency, and leads to a internal quantum efficiency even higher than 100% due to the carrier recycling effect [110, 111]. However, the cost of this design lies on the challenging material growth and the increased forward voltage [112, 113]. Compared to the cascaded active region, it is less difficult to increase the hole penetration depth by Mg-doped quantum barriers where a moderate Mg dosage level is required [114–117]. Kuo et al. initiated the GaN/InGaN-type last quantum barrier to promote the hole injection efficiency [41], and the experimental works have also been conducted and reported by several groups [42–44]. The GaN/InGaN-type last quantum barrier further evolves into the GaN/InGaN supperlattice as the hole reservoir layer [118]. Although the GaN/InGaN-type and GaN/InGaN-superlattice-type last quantum barriers show the advantage in increasing the hole injection capability both numerically and experimentally, the physical interpretations, nevertheless, are still unclear so far. Besides structurally modifying devices, the hole injection can be manipulated by material engineering, such that Li et al. reveal that a longer hole penetration depth can be enabled by the V-shape pits provided that the pit size is fully optimized [119].

To summarize, we have reviewed the most adopted methods to increase the hole injection efficiency for InGaN/GaN LEDs. One can promote the hole transport by reducing the valence band barrier height of the p-EBL and manipulating the hole transport mechanism, e.g., through the subband tuning effect. Besides, the hole injection can also be enhanced by increasing the kinetic energy of holes, which can be achieved by the hole accelerator. In the meanwhile, the improved doping efficiency for the p-GaN layer offers another design strategy for enhancing the hole injection efficiency, such as the 3DHG structure and the hole modulator. In addition to increasing the hole injection across the p-EBL, it is also essentially important to homogenize the hole distribution within the active region so that the holes can penetrate into those deep quantum wells close to the n-GaN layer.

3.3 Improving the quantum efficiency through screening the polarization effect in the quantum wells

3.3.1 Screening the polarization effect by engineering the energy band for the active region As has been well known, InGaN/GaN MQWs grown along the [0001] orientation feature a very strong polarization field, which disables the flat band condition for the quantum wells and quantum barriers. More importantly, the polarization-induced electric field spatially separates the electron and hole wave functions, well known as the QCSE [12, 13]. Therefore, in order to increase the radiative recombination rate, it is vital to suppress the polarization effect in the quantum wells. The QCSE can be alleviated by using very thin quantum wells. However, the thin quantum wells cause the poor electron capture efficiency [120]. Currently, the most effective way to screen the polarization effect in the quantum wells is to adopt the non-polar and semi-polar LED architectures [121, 122]. Until now, (11–20) A-plane and (1–100) M-plane are the most popular non-polar growth planes, on which the quantum wells can be completely free from any polarizations. Successful demonstrations of non-polar LEDs and laser diodes have been presented by quite a few groups. By using the photoluminescence method, Craven et al. conclude that the A-plane GaN/AlGaN quantum well is still able to yield the emission even the quantum well width is beyond 5 nm while the C-plane GaN/AlGaN quantum well fails [123]. This indicates the advantage of growing quite thick non-polar quantum wells over those grown on the [0001]-oriented plane. Chitnis et al. grow and fabricate the A-plane InGaN/GaN MQW LED on the R-plane sapphire substrates [124], and their experimental results evidence the absence of the polarization field in the quantum wells. However, a huge blue shift of the peak emission wavelength (covering the 425–450 nm within 20–500 A cm^{-2}) is observed, which is attributed to the band filling effect due to the InN fluctuation in the quantum wells. The InN fluctuation can be reduced by growing A-plane InGaN/GaN LED on the A-plane GaN substrate [125], and the electroluminescence peak position of 413.5 nm is independent of the drive current indicating the uniform InN composition and the absence of the polarization effect in the quantum wells. Later on, the first blue M-plane InGaN/GaN LED with the peak emission wavelength of 450 nm is grown by Chakraborty et al. on the free-standing M-plane GaN substrate [126]. Then, the peak emission wavelength that further extends to the range between 460 and 500 nm is achieved by the M-plane InGaN/GaN LED on the defect-free M-plane GaN substrate and nearly blueshift-free emission is observed in all LEDs within the current density of 1–400 A cm^{-2} under the pulsed operation [127]. Detchprohm et al. report the realization of the green A-plane InGaN/GaN LED with the peak emission wavelength of 520 nm on the A-plane sapphire substrate [128].

Furthermore, the work by Detchprohm et al. has also suggested that the A-plane InGaN/GaN LED on the R-plane sapphire substrate has a high threading dislocation density of 2×10^{10} cm^{-2}, which makes the free-standing GaN as the optimum candidate for growing the high-quality nonpolar InGaN/GaN MQWs [128]. Free-standing GaN substrates nevertheless increase the cost for growing the InGaN/GaN quantum wells. Therefore, many efforts have also been invested to explore the alternatives to screen the polarization effect in the [0001] quantum wells. Recently, by properly alloying the ternary and quaternary quantum barriers, the polarization-matched InGaN/InAlN and InGaN/InAlGaN quantum well/quantum barrier structures have been proposed and studied both experimentally and numerically [62, 63, 129, 130].

However, the epitaxial growth of InAlGaN and InAlN is difficult considering the different growth temperatures for simultaneously incorporating the In and Al atoms into the crystal. Another convenient way to suppress the polarization effect in the blue quantum wells is to adopt the staggered quantum wells [131–133]. Zhao et al. have experimentally proved the effectiveness of the staggered quantum wells in reducing the polarization and charge separation in the green InGaN/GaN quantum wells (520–525 nm) [134], and the staggered quantum wells are also useful in the 530 nm regime as reported by Park et al. [135].

3.3.2 Screening the polarization effect by Si-doped quantum barriers It is also suggested that the polarization effect in the quantum wells can be well screened by Si doping the quantum barriers [15], such that the free electrons released by the Si dopants in the quantum barriers are able to screen the polarization-induced interface charges in the quantum wells. The impact of the Si doping concentration on the strain and cracking for the GaN layer has been thoroughly studied by Romano et al. [136]. It shall be noted the quantum barrier thickness is much smaller than the threshold thickness that is 2 μm when the Si doping concentration is 2×10^{19} cm^{-3} in the GaN layer. Meanwhile the first-principle calculations show the lattice constant has negligible changes if the Si atoms replace the Ga atoms in the GaN film. In addition, the X-ray diffraction conducted by Wu et al. indicate that the crystal and interfacial quality of the InGaN/GaN architectures can be significantly improved by Si-doping the quantum barriers [137] and the same conclusions are also made by Lee et al. [138]. As the result, the quantum barriers doped by Si dopants have the superiority over those without introducing Si dopants.

Despite the advantages of the Si-doping feature in the quantum barriers, the Si-doped quantum barriers hinder the hole injection [139]. Therefore, we propose the Si-step-doped quantum barriers in increasing the hole injection efficiency [140]. More importantly, our results show that the doping position in the quantum barrier is extremely important for more effectively screening the polarization effect in the quantum wells. The recommended device architecture with Si-step-doped quantum barriers is shown in Fig. 12(c) whereas Fig. 12(a) and (b) have the unintentionally n-type quantum barriers and Si fully doped

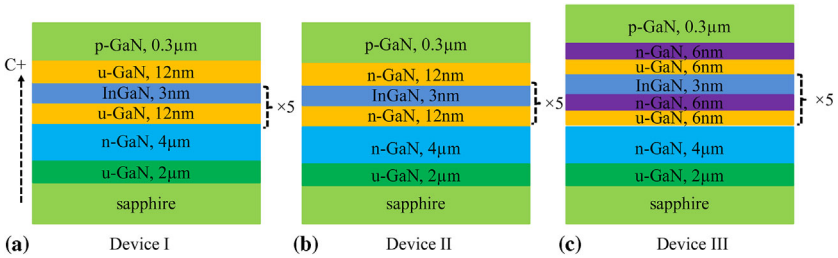

Figure 12 Schematic device architectures for (a) reference LED device: Device I, (b) LED device with Si fully doped quantum barriers: Device II, and (c) proposed LED device with Si-step-doped quantum barriers: Device III. The thickness for each layer is also presented in the figures. Reproduced from Ref. [140], with the permission of Optical Society of America.

quantum barriers, respectively. The Si concentration in the quantum barriers is selectively doped at a high level of $2.6 \times 10^{18}\,\mathrm{cm}^{-3}$. According to our report, the ionized Si dopants play very crucial role in suppressing the polarization effect in the quantum wells, and this is calculated by using APSYS and explained by Fig. 13(a)–(d), respectively. The device mesa in this study is $350 \times 350\,\mu\mathrm{m}^2$.

Figure 13(a) shows that Si-step-doped quantum barriers are even better than the Si fully doped quantum barriers in reducing the polarization-induced electric field intensity in the quantum well. Device II is effective in reducing the polarization field at site B rather than at site A, the reason behind which is illustrated in Fig. 13(c). The additional positively ionized Si dopants plus the polarization-induced interface charges (positive) at site A increase the net charge density, and this is responsible for the increased field intensity. On the other hand, the positively ionized Si dopants compensate the polarization-induced interface charges (negative) at site B and this leads to the reduction of the polarization induced electric field for both Devices II and III. However, the absence of the ionized Si dopants at site A in Device III is helpful to maintain a small field intensity as shown in Fig. 13(a) and (d), respectively. Figure 13(e) presents the EQE and the optical power in terms of the injection current for the three devices, from which we can see that Devices II and III can produce stronger optical power than Device I due to the screened polarization field in the quantum wells. Meanwhile, the largest polarization screening effect in the quantum wells for Device III leads to the strongest optical performance. Hence, the ionized Si dopants strongly influence the polarization field profiles, and the Si-doped position in the quantum barriers is essentially critical in better screening the polarization effect in the quantum wells. For the [0001]-oriented quantum well structures, we have recommended the doping configuration that is shown in Fig. 12(c).

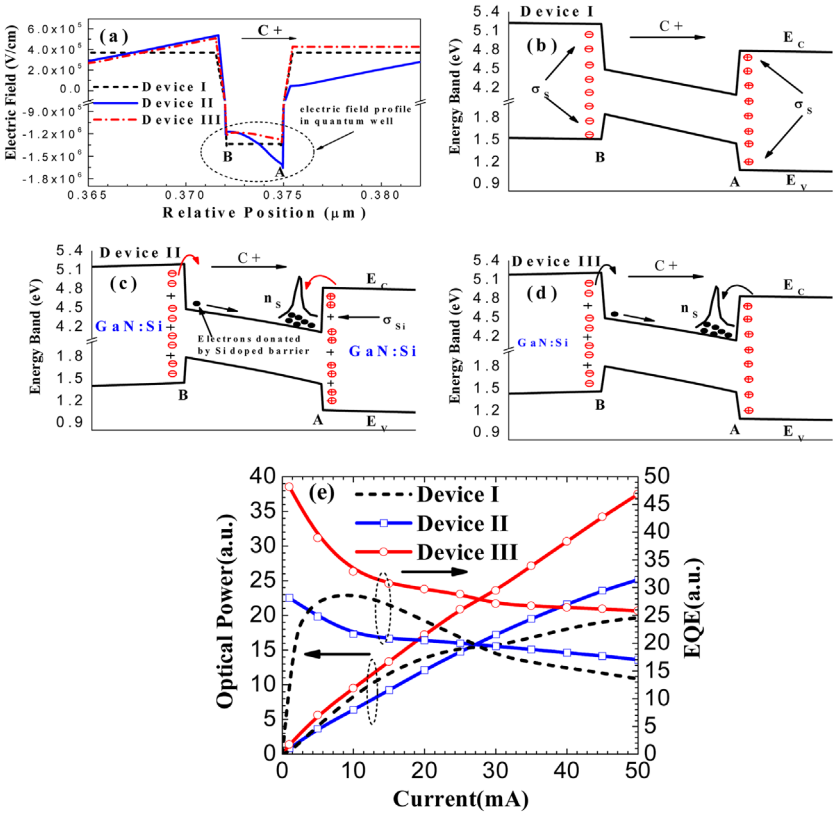

Figure 13 (a) Calculated electric field profiles in the last quantum well for the three devices. The charge profiles for (b) Device I, (c) Device II, (d) Device III, respectively, and (e) experimentally measured EQE and optical power in terms of the current. Data collected at 50 mA. Reproduced from Ref. [140], with the permission of Optical Society of America.

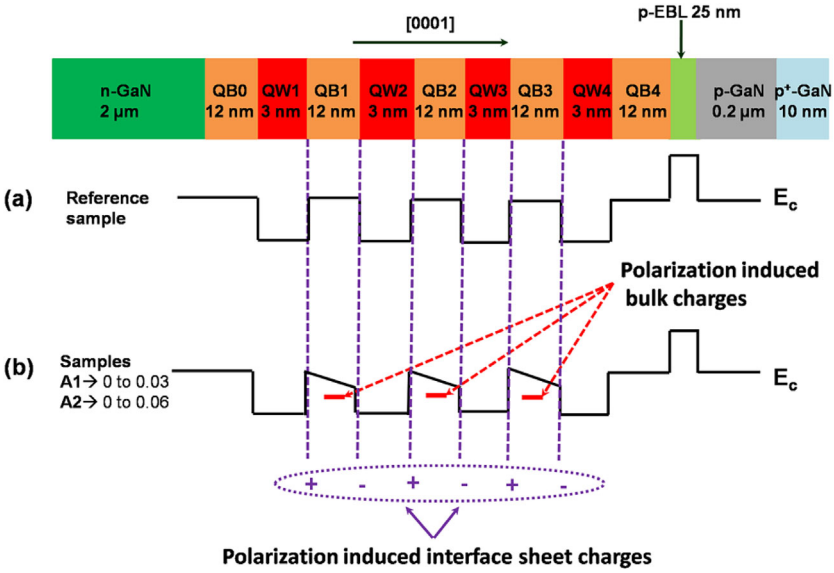

Figure 14 Schematic device architectures and the conduction band diagrams for (a) reference sample which has $In_{0.15}Ga_{0.85}N$ and GaN as the quantum wells (QWs) and quantum barriers (QBs), respectively, and (b) samples A1 and A2, which have InGaN as the quantum barriers, and the InN composition is linearly increased from 0.0% to 3.0% and from 0.0% to 6.0% for samples A1 and A2, respectively. Here, p-EBL denotes the p-type electron blocking layer and the thickness of each layer is shown in the figure. Reproduced from Ref. [49] with the permission from AIP publishing.

Similarly, the role of ionized Si-dopants in screening the polarization effect is then also reported by Kim et al. in 2015 [141], and they recommend the same doped position for [0001] InGaN/GaN LEDs as shown in Fig. 12(c).

3.3.3 Polarization self-screening effect in quantum wells Inspired by the work of Ref. [140], we further propose and develop the polarization self-screening effect such that the polarization effect in the quantum wells can be self-screened by the polarization-induced bulk charges in the quantum barriers [49]. The device architectures to realize the polarization self-screening effect are depicted in Fig. 14(a) and (b). The quantum wells are grown along the [0001] orientation, and this results in the polarization-induced sheet charges at the quantum well/quantum barrier interface, as can been seen from Fig. 14. Meanwhile, once the InN composition in the quantum barriers is linearly increasing along the [0001] orientation, the negative polarization-induced bulk charges in the quantum barriers are generated [99, 102]. The charge density is calculated and demonstrated in Table 2. The details in calculating the polarization-induced bulk charges can be found in Ref. [49]. As the grading level in the quantum barriers for sample A2 is larger than sample A1, therefore, more charges can be produced for sample A2.

In order to demonstrate the self-screening capability, we both experimentally measure the peak wavelength in terms of the injection current density (Fig. 15(a)) and numerically calculate the field profiles in the quantum well region (Fig. 15(b)). The self-screening effect to the polarization in the quantum wells is reflected by the reduced peak emission wavelength when comparing samples A1, A2, and the reference sample. According to Table 2, sample A2 has more polarization-induced bulk charges than sample A1, and therefore sample A2 is better than sample A1 in further reducing the polarization in the quantum wells. Thus, sample A2 has the shortest peak emission length. The theoretical proof is shown in Fig. 15(b), agreeing well with the experimental measurement in Fig. 15(a) that samples A1 and A2 can better decrease the polarization level in the quantum wells than the reference sample with sample A2 best screening the polarization.

We have also obtained the same results (Fig. 16(a) and (b)) if the InN composition is graded in the opposite than for samples A1 and A2, such that the InN composition is linearly decreased from 3.0% to 0.0% for sample B1 and from 6.0% to 0.0% for sample B2. In this case, the quantum barriers possess the positive polarization-induced charges while the charge density is unchanged as shown in Table 2. However, we grew the LED structures in different epitaxial runs, and this might cause the slight fluctuations in the InN

Table 2 Calculated polarization-induced interface charges and bulk charges in the MQW region for the reference sample, samples A1 and A2.

σ_S^{Pol}	$In_{0.15}Ga_{0.85}N/GaN$ $0.55 \times 10^{17}\,m^{-2}$	$In_{0.15}Ga_{0.85}N/In_{0.03}Ga_{0.97}N$ $0.44 \times 10^{17}\,m^{-2}$	$In_{0.15}Ga_{0.85}N/In_{0.06}Ga_{0.97}N$ $0.33 \times 10^{17}\,m^{-2}$
ρ_B^{Pol}	$In_{0.03}Ga_{0.97}N \leftrightarrow GaN$ within 12 nm $9.19 \times 10^{23}\,m^{-3}$		$In_{0.06}Ga_{0.94}N \leftrightarrow GaN$ within 12 nm $1.84 \times 10^{24}\,m^{-3}$

A 40% polarization level is assumed considering the dislocation generation during the epitaxial growth process. Reproduced from Ref. [49], with the permission of AIP publishing.

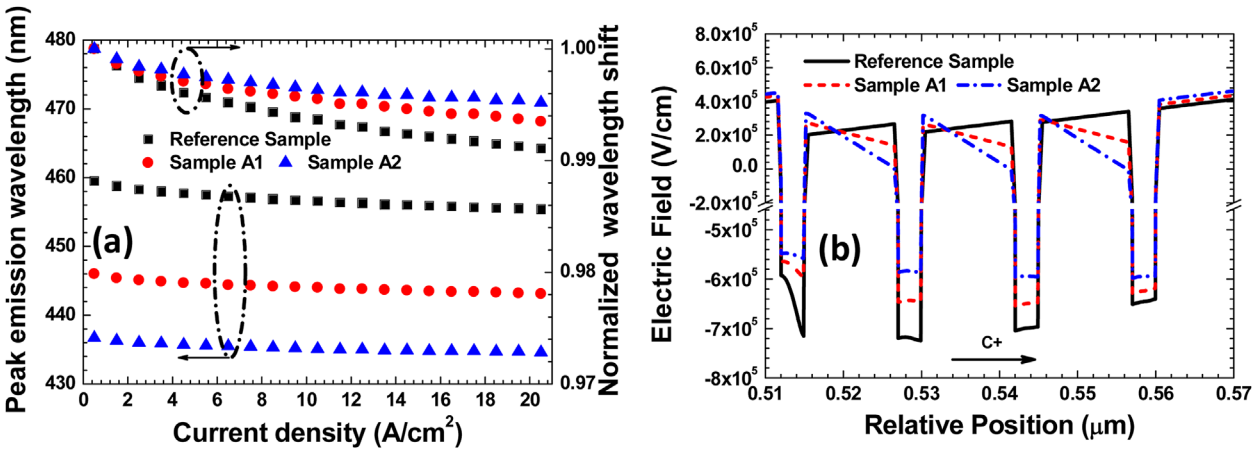

Figure 15 (a) Experimentally measured peak emission wavelength as a function of the current density and (b) numerically calculated polarization-induced electric field profiles in the quantum wells for the reference sample, samples A1 and A2, respectively. The electric field profiles are collected at 0 V. Reproduced from Ref. [49], with the permission of AIP publishing.

incorporation efficiency, and the peak emission wavelengths, therefore, vary between sample A1 and sample B1, sample A2, and sample B2. Nevertheless, the wavelength variations do not change our conclusion that the polarization effect can be self-screened by the polarization-induced bulk charges in the quantum barriers. It shall be noted that the polarization self-screened MQW structure is free from any hole blocking effect [49].

To summarize, in this subsection, we have reviewed the approaches employed to screen the polarization effect, which often appears in the, e.g., [0001] oriented III–V nitride quantum wells. One can engineer the energy band for the quantum wells, such as nonpolar/semipolar structures, polarization-matched quantum well/quantum barrier structures. An easier way is to adopt Si-doped quantum barriers, and more importantly, we have demonstrated the importance of the ionized Si dopants in affecting the polarization-induced electric field. We also recommend the preferable Si-doping profiles for the [0001]-oriented quantum well. In addition, the ionized dopants can be replaced by the polarization induced bulk charges which are obtained by grading the alloy composition in the quantum barriers, and by doing so, we obtain the polarization self-screening effect.

3.4 Current spreading layers for nitride light-emitting diodes Current crowding strongly deteriorates the device performance for III–V nitride-based LEDs, which induces a high local current density and local heat [142, 143], thus causing a substantially non-uniform light distribution and also causes the efficiency droop [16, 144, 145]. Compared with electrons, the holes are even much easier to crowd due to the worse electrical conductivity for the p-GaN layer. In order to better demonstrate the flowing current, a schematic device architecture and a simplified equivalent circuit for the III nitride-based LED with a lateral current injection scheme are

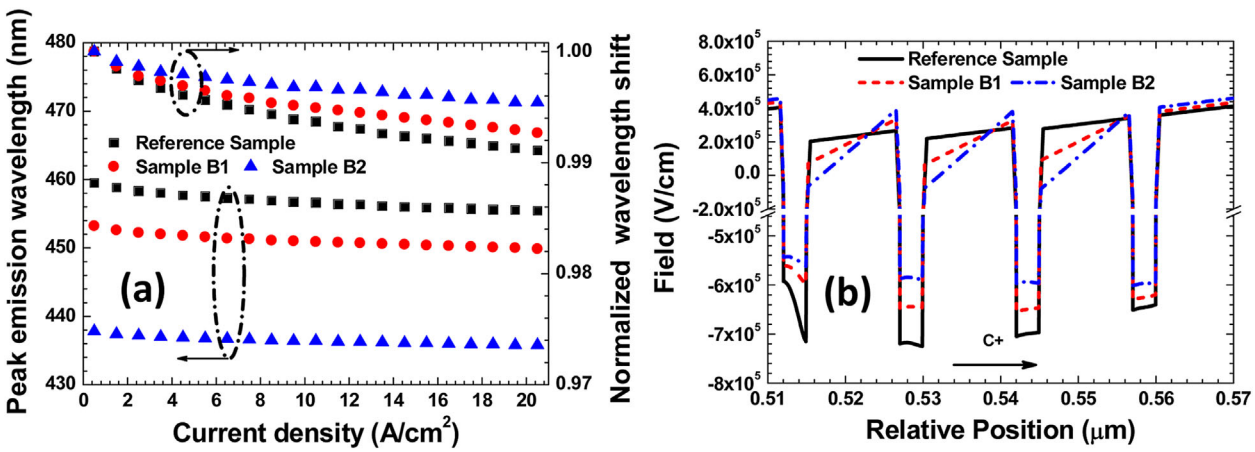

Figure 16 (a) Experimentally measured peak emission wavelength as a function of the current density and (b) numerically calculated polarization-induced electric field profiles in the quantum wells for the reference sample, samples B1 and B2, respectively. The InN composition is linearly decreased in samples B1 and B2. The electric field profiles are collected at 0 V.

shown in Fig. 17(a) and (b), respectively [146]. The resistances of the transparent current spreading layer (TCL) and n-GaN layer are represented by R_{TCL}, R_{n-GaN2}, and $R_{n\text{-}GaN3}$, respectively. The total vertical resistance for each branch is denoted as R_x, and $R_x = R_{p\text{-}GaN} + R_{MQW} + R_{n\text{-}GaN1} + R_{TCL/p\text{-}GaN}$, in which the resistances of p-GaN, MQW, and n-GaN are denoted as $R_{p\text{-}GaN}$, R_{MQW}, and $R_{n\text{-}GaN1}$, respectively, while the interfacial resistance between TCL and p-GaN is $R_{TCL/p\text{-}GaN}$. The total current is divided into I_0, I_1, and I_2. According to Fig. 17(b), the relationship among I_0, I_1, and I_2 is obtained and shown in Eqs. (2) and (3). Thus, in order to increase I_1, one can either increase R_x or reduce R_{TCL}. Moreover, a reduced R_{TCL} also benefits I_2. However, the TCL (e.g., ITO) thickness normally is 100–200 nm, while the n-GaN layer is of 2–4 μm, and as the result, the area of the cross section through which the current flow for TCL is smaller than that for n-GaN layer, hence $R_{n-GaN2} < R_{TCL}$. Note that if the R_{TCL} is tremendously reduced (e.g., thick metal mirror layer for flip-chip LEDs), I_2/I_0 will be larger than 1 that means the current crowds at the edge of the mesa. Nevertheless, according to Eq. (3), a properly increased R_x (e.g., by a current blocking layer) and a properly reduced R_{TCL} enable an even current distribution. The conclusions we make here are consistent with the reports by Guo et al. [17] and Ryu et al. [145].

$$\frac{I_1}{I_0} = \frac{1}{1 + \frac{R_{TCL} + R_{n\text{-}GaN2}}{R_x}}, \tag{2}$$

$$\frac{I_2}{I_0} = 1 + \frac{R_{n\text{-}GaN2} - R_{TCL}}{R_x + R_{TCL}} = \frac{R_{n\text{-}GaN2} + R_x}{R_x + R_{TCL}}. \tag{3}$$

The common way to increase the R_x is to make certain layers resistive by, for example, selectively ion-implanting the p-GaN layer [147, 148] or by embedding the insulating layer (e.g., Al_2O_3, SiO_2) between the p-GaN layer and the p-contact [149, 150]. Lin et al. selectively cap the p-GaN layer with the Ti metal film while the Ti diffusion can reduce the hole concentration and make the p-GaN layer locally high resistive [151]. By inductively coupled plasma (ICP) etching, Kuo et al. selectively produce nitrogen vacancies to compensate the holes in the p-GaN layer [152]. Another convenient way to properly increase R_x is to *in situ* grow the barrier junction in the p-GaN layer. Liu et al. propose the short-period i-InGaN/p-GaN superlattice [153, 154], and they make use of the energy band discontinuity between the InGaN and GaN layers to modify R_x. Recently, we have developed the $(p\text{-GaN/n-GaN/p-GaN})_x$ current spreading layer [155], and such design avoids the growth difficulty in growing the lattice-mismatched materials. The schematic device architectures for the studied devices are shown in Fig. 18. In our design, we select two p-GaN/n-GaN/p-GaN (PNP-GaN) junctions, i.e., p-GaN/n-GaN/p-GaN/n-GaN/p-GaN (PNPNP-GaN). The thickness of the n-GaN layer has to be properly selected so that the n-GaN layer can be completely depleted at the equilibrium state so that each PNP-GaN junction consumes no bias, and this will not increase the forward bias. Meanwhile, Fig. 18(b) and (c) illustrates the calculated energy bands for the reference LED and the PNPNP-GaN LED. The current spreading effect can be improved for the PNPNP-GaN LED thanks to the junction barriers by the PNPNP-GaN structures. As the result, the quantum efficiency is experimentally enhanced by 16.98% and 14.37% at 20 and 100 mA (see Fig. 18(d)), respectively. Note that the device mesa size is $350 \times 350\ \mu m^2$ for the LED devices. According to Eq. (3),

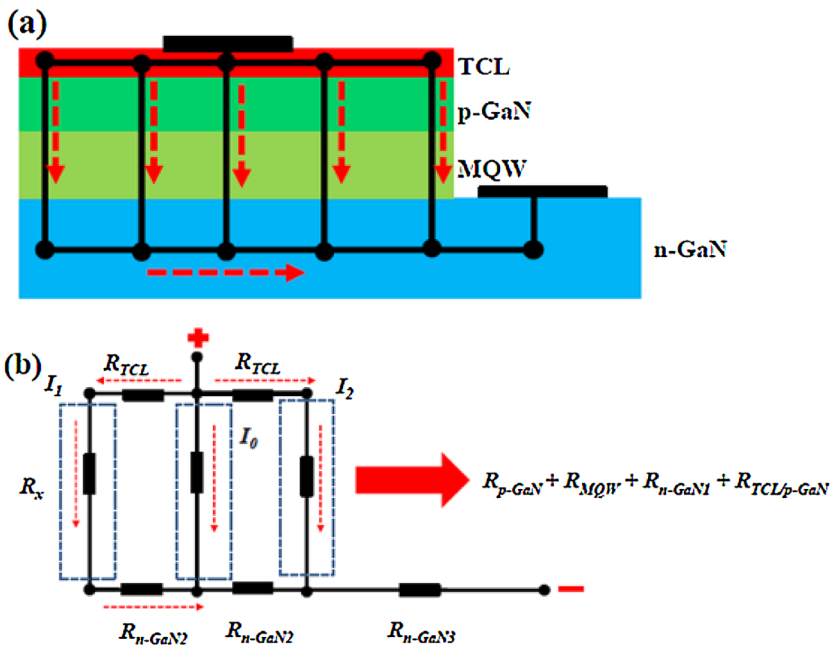

Figure 17 (a) Schematic device architecture with current flow paths and (b) simplified equivalent circuit for InGaN/GaN LEDs grown on insulating substrates. After Ref. [146].

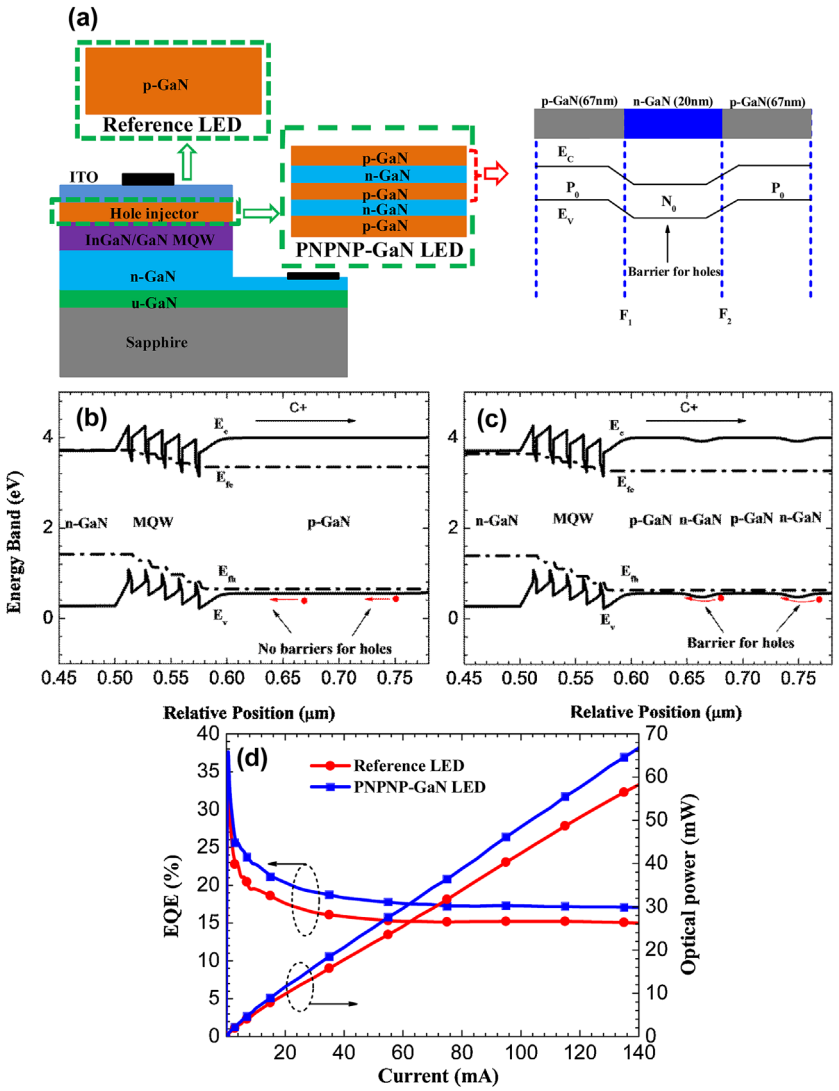

Figure 18 (a) Device architectures for the reference LED and the PNPNP-GaN LED (the schematic energy band for the PNP-GaN junction is also demonstrated). Numerically calculated energy bands for (b) the reference LED and (c) PNPNP-GaN LED. (d) Experimentally measured EQE and the optical power in terms of the current for the reference LED and the PNPNP-GaN LED. Reproduced from Ref. [155], with the permission of Optical Society of America.

by making the n-GaN layer more resistive, the current can better distribute to the edge of the mesa, and for that purpose, we have also suggested the (n-GaN/p-GaN/n-GaN)$_x$ junction embedded in the n-GaN layer [156], which shows 19.90% and 23.77% enhancement for quantum efficiency at 20 and 100 mA (chip size of $350 \times 350\ \mu m^2$), respectively. However, the forward voltage of that proposed device is increased, e.g., by ~0.6 V at 20 mA, which is due to the non-optimized p-GaN thickness.

As mentioned, another approach to improve the current spreading is to reduce the R_{TCL}. Therefore, the n^+-GaN/p^+-GaN tunnel junction is demonstrated to improve the current spreading [157–161]. However, the carrier interband tunneling process requires a strong electric field in the tunnel junction, which is merely determined by the doping concentration in the n^+-GaN/p^+-GaN junction. In order to further promote the carrier interband tunneling efficiency, we propose the polarization tunnel junction, i.e., n^+-GaN/InGaN/p^+-GaN junction [162]. The polarization-induced electric field in the InGaN thin layer (3 nm was chosen in our work) follows the same direction as the built-in electric field in the junction, and this results in a higher field intensity favoring the interband tunneling process [163]. Therefore, compared to the n^+-GaN/p^+-GaN tunnel junction, the n^+-GaN/InGaN/p^+-GaN tunnel junction reduces the forward bias by ~0.7 V (the mesa size is $350 \times 350\ \mu m^2$). Meanwhile, the polarization tunnel junction improves the hole injection which is effective in improving the external quantum efficiency.

To summarize, we have proposed the model to design LED devices with the improved current spreading effect. The model can well interpret the current technologies that are adopted to improve the current spreading. On one hand, the current can be evenly distributed by properly increasing the vertical resistance (R_x), e.g., selectively making the p-GaN layer underneath the p-electrode high resistive or adopting PNP-GaN junctions. On the other hand, the current crowding can be alleviated by properly reducing the resistance of the current spreading layer (R_{TCL}), i.e., using tunnel junctions. Besides, properly increasing the resistance

of the n-GaN layer ($R_{n\text{-}GaN2}$) is also helpful to improve the current spreading, such as reducing the n-GaN doping concentration or using NPN–GaN junctions.

3.5 Reducing the defect density to make better use of carriers for high radiative recombination rate To date, there is no consensus if the defect-related recombination is responsible for the efficiency droop [8, 22–25, 164]. However, it is straightforward that, by reducing the defect-related recombination, the LED quantum efficiency can be enhanced. An effective way to suppress the impact of defects on the SRH recombination (e.g., DADR) is to introduce the V-defects. Theoretical and experimental studies indicate that V-defects can screen the carriers from the non-radiative recombination centers [165–169]. However, the role of the V-defects in affecting the quantum efficiency for InGaN/GaN LEDs is arguable till now [170–172]. Moreover, it is also essential to improve the crystal quality and suppress the defect-related recombination, such as the InGaN/GaN LED epitaxial growth on the nano-patterned substrate [173]. According to the report in the Ref. [173] by Li et al., the nano-patterned substrate doubles the internal quantum efficiency of the green InGaN/GaN LED, and this is attributed to the 44% lower dislocation density which is observed through the transmission electron microscopy.

3.6 High radiative recombination efficiency by suppressing the Auger recombination in nitride light-emitting diodes As discussed earlier in this work, the Auger recombination consumes carriers, and thus the IQE can be promoted if the Auger recombination can be minimized. The Auger recombination scales to the cubic power of the carrier density, which indicates that a suppressed Auger recombination can be obtained by reducing the carrier density in the quantum wells. Chang et al. have numerically concluded that merely increasing the quantum well number makes little impact in reducing the Auger recombination [174]. Their conclusions make sense if considering the limited hole injection depth into the quantum wells. Given that the polarization-induced electric field deforms the quantum well and causes a strong local carrier accumulation, Chang et al. propose and demonstrate the polarization matched InGaN/AlGaInN quantum well architectures while the quantum well thickness can be

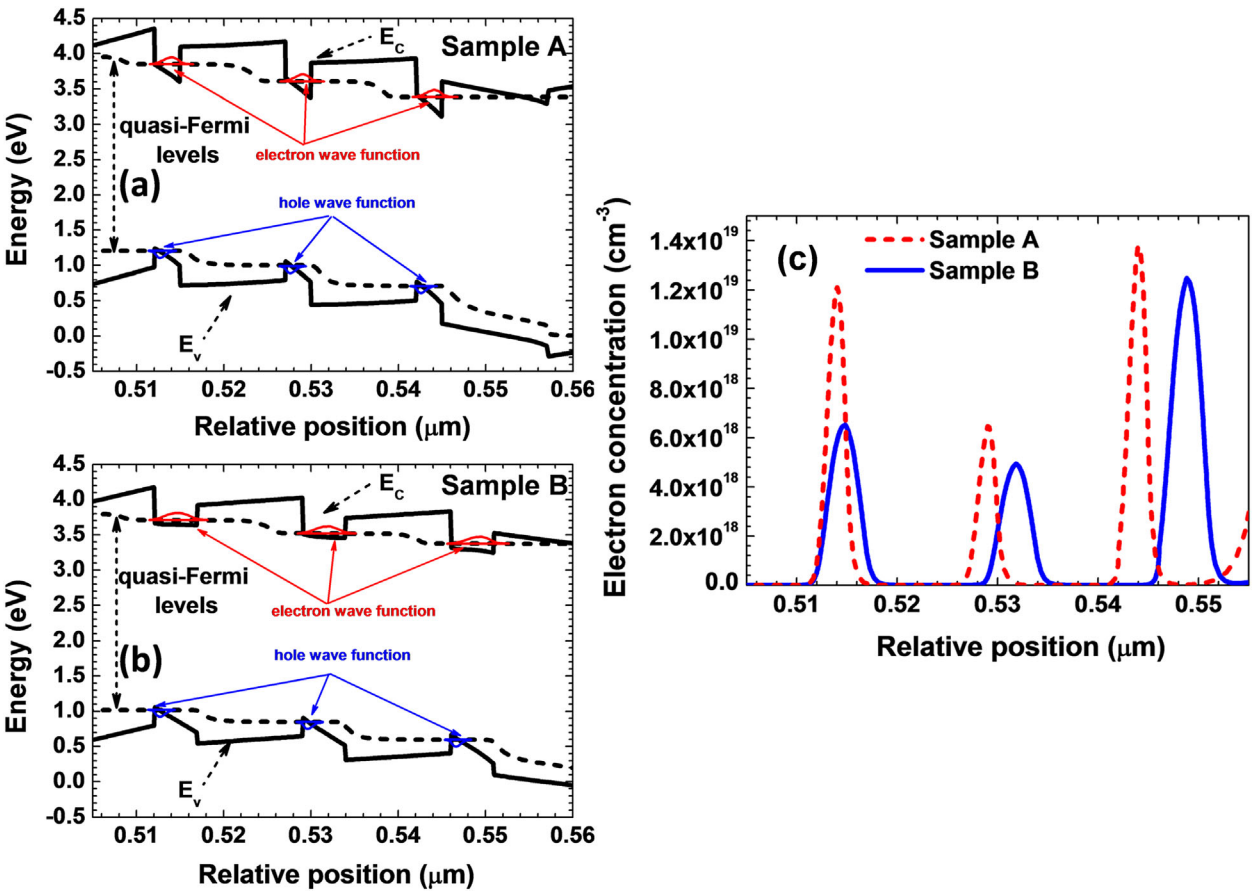

Figure 19 Numerically calculated energy band diagrams for (a) sample A and (b) sample B. (c) Electron density profiles for both samples. Data are collected at 140 A cm^{-2}. C1 and HH2 subband wave functions are also included in (a) and (b), E_C and E_V present the conduction band and the valence band, respectively. Reproduced from Ref. [176], with the permission of AIP publishing.

properly increased [174]. The proposed design by Chang et al. on one hand alleviates the polarization level and flattens the quantum well energy band, and on the other hand, reduces the local carrier density. As a result, the Auger recombination is suppressed. The report by Chang et al. is consistent with the results by Vaxenburg et al. and Kioupakis et al. [33, 175].

We have also proposed a gradient InN composition in the quantum wells to suppress the Auger recombination for blue InGaN/GaN LEDs [176]. Two blue InGaN/GaN LEDs are grown by the MOCVD technology and the peak emission wavelength for the two grown LEDs is ~450 nm. Sample A has the conventional quantum well structures such that the $In_{0.15}Ga_{0.85}N$/GaN architecture has the quantum well and quantum barrier thicknesses of 3 and 12 nm, respectively. Nevertheless, the InN composition in sample B is linearly decreased from 15% to 8% with the thickness of 5 nm range to avoid the wavelength variation, i.e., $In_{0.15\rightarrow0.08}Ga_{0.85\rightarrow0.92}N$/GaN. The energy band diagrams at 140 A cm^{-2} for the two LED samples are shown in Fig. 19(a) and (b), respectively, along with which also presents the C1 and HH1 subbands. Clearly, we can see from Fig. 19(b) that the conduction band for sample B is flattened and the electron can be more evenly distributed in each quantum well, which is also reflected by the electron density profiles for samples A and B as illustrated in Fig. 19(c). The electrons are less locally accumulated in the quantum wells, and this is helpful to suppress the Auger recombination.

In order to probe the impact of the proposed quantum well structure on reducing the Auger recombination rate, we have both numerically calculated and experimentally measured the optical output power and the EQE as the function of the injection current (Fig. 20(a) and (c)). Investigations into Fig. 20(a) and (c) tell that sample B improves the device performance compared to sample A, and the experimentally measured optical output power for sample B at the current density level of 150 A cm^{-2} is increased by 29.39%. More importantly, according to Fig. 20(b) and (d), the efficiency droop for sample B is reduced both numerically and experimentally. The experimental droop level decreases from 39.23% to 31.83% at 150 A cm^{-2}. The enhanced device performance and the reduced efficiency droop for sample B are well attributed to the suppressed Auger recombination in the quantum wells, which have also been calculated and demonstrated in Fig. 20(e), according to which the rising Auger recombination overwhelms the radiative recombination for sample A when the current density exceeds 150 A cm^{-2}. However, the Auger recombination is always lower than the radiative recombination for sample B. Our study supports that the Auger recombination is one of the reasons causing the efficiency droop.

Unlike the SRH recombination rate that can be solved by reducing the SRH recombination coefficient through either improving the crystal quality or screening dislocation from carriers, the Auger recombination coefficient is the intrinsic material property that is strongly decided by the energy band gap. Thus, the effective way to suppress the Auger-recombination-caused carrier loss is to achieve the flat band condition and makes the carriers more uniformly distributed within the quantum wells. In this section, we have reviewed some approaches which realize the flat band condition. We also believe the Auger recombination can be suppressed by employing the non-polar quantum wells. Meanwhile those semi-polar quantum wells with a slight [000-1] properties, e.g., (11–22) quantum wells reported by Ji et al. [122], are also

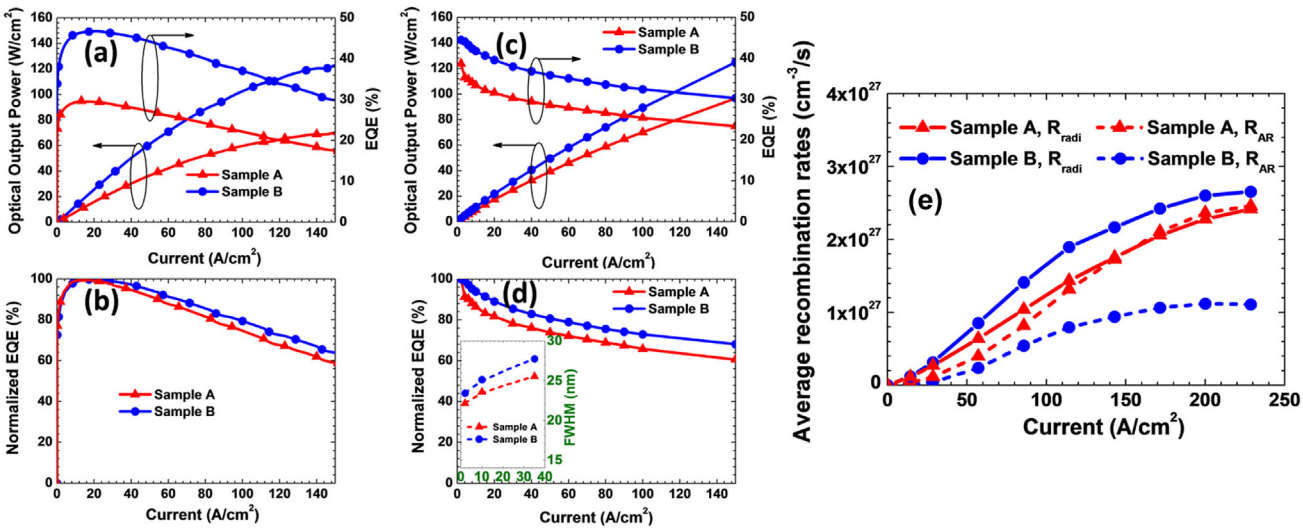

Figure 20 (a) Numerically calculated optical output power and the EQE for samples A and B, (b) numerically calculated and normalized EQE for samples A and B, (c) experimentally measured optical output power and EQE for samples A and B, (d) experimentally measured and normalized EQE for samples A and B, and (e) numerically calculated radiative recombination rate (R_{radi}) and Auger recombination rates (R_{AR}) in terms of the injection current density for samples A and B. Inset figure in (d) shows the full width at half maximum (FWHM) at different current density levels for samples A and B. Reproduced from Ref. [176], with the permission of AIP publishing.

favorable to obtain the flat band condition and promise the suppressed Auger recombination.

4 Conclusions and future outlook Improving the IQE for III nitride-based LEDs is vitally important for expanding the solid-state lighting market. The LEDs face the challenges of unsatisfied carrier injection efficiency, current crowding effect, Auger recombination, defect-induced recombination, and polarization effect, which all take the responsibility for limiting the IQE.

We have reviewed and compared the most recently developed methods to address the issues which hinder the enhancement of the IQE for III–V nitride-based LEDs. In addition, we have also proposed and studied the alternative design strategies. An increase of the electron injection efficiency can be obtained by, e.g., reducing the electron kinetic energy before they enter the active region and/or suppressing the local electron accumulation level at the interface of the last quantum barrier and the p-EBL. The hole injection efficiency can be promoted, for example, by increasing the hole concentration in the p-GaN layer and/or making hole more energetic. Regarding the polarization screening approaches, we have demonstrated the effect of the ionized dopants in the quantum barriers on screening the polarization effect in the quantum wells, which makes the doped position in the quantum barriers extremely important. The ionized dopants can then be replaced by the polarization induced bulk charges, i.e., polarization self-screening effect. The current crowding effect in the LED devices can be further alleviated by properly varying the resistances in the p-GaN and n-GaN layers, respectively. The radiative recombination efficiency is also affected by the SRH recombination that can be weakened by growing LED epi-wafers on the nano-patterned substrate to improve the crystal quality. Besides, introducing the intentional V-pits with proper size can also screen the carriers from recombining at the non-radiative recombination centers. As is well known, the Auger recombination consumes a large number of carriers especially when the device is biased at a high current injection level, whereas the Auger recombination can be decreased by reducing the local carrier density. A low local carrier density can be obtained if the quantum well reaches the flat band condition, and this can be realized by grading the InN composition for the polar quantum wells.

In this work, various reviewed approaches are effective to improve the IQE for LEDs. However, the origin for the improved device performances has not been well explained for some certain LED architectures, which hence require further investigations. Note, various proposed LED structures were grown by different groups with different epi-growth technologies, and it is difficult to conclude the most useful device structures. It is, therefore, necessary to evaluate the overall quantum efficiency enhancement by incorporating the proposed technologies into a single LED epi-structure.

In addition, most of the reviewed work is conducted on the blue InGaN/GaN LEDs. It is very interesting to expand the demonstrated designs to other import wavelengths such as green and deep ultraviolet (DUV) emissions. As is well known, green InGaN/GaN LEDs also suffer from the polarization fields in the polar quantum wells, Auger recombination, insufficient electron and hole injection, etc.

The low IQE also strongly influences the DUV LEDs, which have found the great potential of being used in skin cure, dissociation of the pollutant materials, semiconductor lighting, etc. [177]. The lack of indium in the quantum wells makes the DUV LEDs more sensitive to the threading dislocations. Meanwhile, the more resistive AlGaN layers result in a serious current crowding effect and the [0001]-oriented quantum wells also features the strong polarization-induced electric field. Besides, the low carrier injection efficiency is another issue we have to solve [178]. Hence, we believe that the proposed device architectures in this work are promising and also applicable to DUV LEDs.

Acknowledgements This work is supported by Natural Science Foundation of China (Project No. 51502074). The authors would also like to thank for the financial support from NRF-RF-2009-09, NRF-CRP-6-2010-02, and A*STAR of Singapore. H.V.D. acknowledges additional support from ESF-EURYI and TUBA-GEBIP.

References

[1] S. T. Tan, X. W. Sun, H. V. Demir, and S. P. DenBaars, IEEE Photon. J. **4**, 613 (2012).
[2] S. Pimputkar, J. S. Speck, S. P. Denbaars, and S. Nakamura, Nature Photon. **3**, 180 (2009).
[3] H. P. Maruska and J. J. Tietjen, Appl. Phys. Lett. **15**, 327–329 (1969).
[4] Nakamura, T. Mukai, M. Senoh, and N. Iwasa, Jpn. J. Appl. Phys. **31**, L139 (1992).
[5] H. Amano, M. Kito, K. Hiramatsu, and I. Akasaki, Jpn. J. Appl. Phys. **28**, L2112 (1989).
[6] S. Nakamura, Jpn. J. Appl. Phys. **30**, L1705 (1991).
[7] H. Amano, N. Sawaki, I. Akasaki, and Y. Toyoda, Appl. Phys. Lett. **48**, 353 (1986).
[8] J. Piprek, Phys. Status Solidi A **207**, 2217 (2010).
[9] H.-Y. Ryu, H.-S. Kim, and J.-I. Shim, Appl. Phys. Lett. **95**, 081114 (2009).
[10] J. Piprek, Nitride Semiconductor Devices Principles and Simulation (WILEY-VCH Verlag GmbH & Co. KGaA, Weinheim, Germany, 2007).
[11] E. E. Mendez, G. Bastard, L. L. Chang, L. Esaki, H. Morkoc, and R. Fischer, Phys. Rev. B **26**, 7101 (1982).
[12] J.-H. Ryou, P. D. Yoder, J. Liu, Z. Lochner, K. Hyunsoo, S. Choi, H.-J. Kim, and R. D. Dupuis, IEEE J. Sel. Top. Quantum Electron. **15**, 1080 (2009).
[13] T. Takeuchi, S. Sota, M. Katsuragawa, M. Komori, H. Takeuchi, H. Amano, and I. Akasaki, Jpn J. Appl. Phys. **36**, L382 (1997).

[14] T. Deguchi, A. Shikanai, K. Torii, T. Sota, S. Chichibu, and S. Nakamura, Appl. Phys. Lett. **72**, 3329 (1998).
[15] V. Fiorentini, F. Bernardini, F. D. Sala, A. D. Carlo, and P. Lugli, Phys. Rev. B **60**, 8849 (1999).
[16] E. F. Schubert, Light-Emitting Diodes, 2nd edn. (Cambridge University Press, Cambridge CB2 8RU, UK, 2006).
[17] X. Guo and E. F. Schubert, J. Appl. Phys. **90**, 4191 (2001).
[18] S. Huang, B. Fan, Z. Chen, Z. Zheng, H. Luo, Z. Wu, G. Wang, and H. Jiang, J. Display Technol. **9**, 266 (2013).
[19] V. K. Malyutenko and S. S. Bolgov, Proc. SPIE **7617**, 76171K (2010).
[20] R. N. Hall, Phys. Rev. **87**, 387 (1952).
[21] W. Shockley and W. T. Read, Phys. Rev. **87**, 835 (1952).
[22] M. F. Schubert, S. Chhajed, J. K. Kim, E. F. Schubert, D. D. Koleske, M. H. Crawford, S. R. Lee, A. J. Fischer, G. Thaler, and M. A. Banas, Appl. Phys. Lett. **91**, 231114 (2007).
[23] X. Shao, H. Lu, D. Chen, Z. Xie, R. Zhang, and Y. Zheng, Appl. Phys. Lett. **95**, 163504 (2009).
[24] J. Hader, J. V. Moloney, and S. W. Koch, Appl. Phys. Lett. **99**, 181127 (2011).
[25] J. Hader, J. V. Moloney, and S. W. Koch, Appl. Phys. Lett. **96**, 221106 (2010).
[26] Y. C. Shen, G. O. Mueller, S. Watanabe, N. F. Gardner, A. Munkholm, and M. R. Krames, Appl. Phys. Lett. **91**, 141101 (2007).
[27] M. Brendel, A. Kruse, H. Jönen, L. Hoffmann, H. Bremers, U. Rossow, and A. Hangleiter, Appl. Phys. Lett. **99**, 031106 (2011).
[28] G. Kim, J. H. Kim, E. H. Park, D. Kang, and B.-G. Park, Opt. Express **22**, 1235 (2014).
[29] R. P. Green, J. J. D. McKendry, D. Massoubre, E. Gu, M. D. Dawson, and A. E. Kelly, Appl. Phys. Lett. **102**, 091103 (2013).
[30] M. Zhang, P. Bhattacharya, J. Singh, and J. Hinckley, Appl. Phys. Lett. **95**, 201108 (2009).
[31] J. Hader, J. V. Moloney, B. Pasenow, S. W. Koch, M. Sabathil, N. Linder, and S. Lutgen, Appl. Phys. Lett. **92**, 261103 (2008).
[32] E. Kioupakis, P. Rinke, K. T. Delaney, and C. G. Van de Walle, Appl. Phys. Lett. **98**, 161107 (2011).
[33] E. Kioupakis, Q. Yan, and C. G. Van de Walle, Appl. Phys. Lett. **101**, 231107 (2012).
[34] J. Cho, E. F. Schubert, and J. K. Kim, Laser Photon. Rev. **7**, 408–421 (2013).
[35] J. Piprek, F. Römer, and B. Witzigmann, Appl. Phys. Lett. **106**, 101101 (2015).
[36] J. Iveland, L. Martinelli, J. Peretti, J. S. Speck, and C. Weisbuch, Phys. Rev. Lett. **110**, 177406 (2013).
[37] D. S. Meyaard, G.-B. Lin, J. Cho, E. F. Schubert, H. Shim, S.-H. Han, M.-H. Kim, C. Sone, and Y. S. Kim, Appl. Phys. Lett. **102**, 251114 (2013).
[38] G. Verzellesi, D. Saguatti, M. Meneghini, F. Bertazzi, M. Goano, G. Meneghesso, and E. Zanoni, J. Appl. Phys. **114**, 071101 (2013).
[39] J. Piprek and Z. M. Simon Li, Appl. Phys. Lett. **102**, 131103 (2013).
[40] D. S. Meyaard, G.-B. Lin, M. Ma, J. Cho, E. F. Schubert, S.-H. Han, M.-H. Kim, H. Shim, and Y. S. Kim, Appl. Phys. Lett. **103**, 201112 (2013).
[41] Y.-K. Kuo, Y.-H. Shih, M.-C. Tsai, and J.-Y. Chang, IEEE Photon. Technol. Lett. **23**, 1630 (2011).
[42] R.-M. Lin, S.-F. Yu, S.-J. Chang, T.-H. Chiang, S.-P. Chang, and C.-H. Chen, Appl. Phys. Lett. **101**, 081120 (2012).
[43] Z. Liu, J. Ma, X. Yi, E. Guo, L. Wang, J. Wang, N. Lu, J. Li, I. Ferguson, and A. Melton, Appl. Phys. Lett. **101**, 261106 (2012).
[44] Z. Kyaw, Z.-H. Zhang, W. Liu, S. T. Tan, Z. G. Ju, X. L. Zhang, Y. Ji, N. Hasanov, B. Zhu, S. Lu, Y. Zhang, J. H. Teng, X. W. Sun, and H. V. Demir, Appl. Phys. Lett. **104**, 161113 (2014).
[45] T. Lu, S. Li, C. Liu, K. Zhang, Y. Xu, J. Tong, L. Wu, H. Wang, X. Yang, Y. Yin, G. Xiao, and Y. Zhou, Appl. Phys. Lett. **100**, 141106 (2012).
[46] H. J. Kim, S. Choi, S.-S. Kim, J.-H. Ryou, P. D. Yoder, R. D. Dupuis, A. M. Fischer, K. Sun, and F. A. Ponce, Appl. Phys. Lett. **96**, 101102 (2010).
[47] S. Choi, M.-H. Ji, J. Kim, H. J. Kim, M. M. Satter, P. D. Yoder, J.-H. Ryou, R. D. Dupuis, A. M. Fischer, and F. A. Ponce, Appl. Phys. Lett. **101**, 161110 (2012).
[48] S. Choi, H. J. Kim, S.-S. Kim, J. Liu, J. Kim, J.-H. Ryou, R. D. Dupuis, A. M. Fischer, and F. A. Ponce, Appl. Phys. Lett. **96**, 221105 (2010).
[49] Z.-H. Zhang, W. Liu, Z. Ju, S. T. Tan, Y. Ji, Z. Kyaw, X. Zhang, L. Wang, X. W. Sun, and H. V. Demir, Appl. Phys. Lett. **104**, 243501 (2014).
[50] Z.-H. Zhang, W. Liu, Z. Ju, S. T. Tan, Y. Ji, X. Zhang, L. Wang, Z. Kyaw, X. W. Sun, and H. V. Demir, Appl. Phys. Lett. **104**, 251108 (2014).
[51] Z.-H. Zhang, Z. Ju, W. Liu, S. T. Tan, Y. Ji, Z. Kyaw, X. Zhang, N. Hasanov, X. W. Sun, and H. V. Demir, Opt. Lett. **39**, 2483–2486 (2014).
[52] V. Fiorentini, F. Bernardini, and O. Ambacher, Appl. Phys. Lett. **80**, 1204–1206 (2002).
[53] S. Chang, Y. Lin, C. Liu, T. Ko, S. Hon, and S. Li, IEEE J. Quantum Electron. **49**, 436–442 (2013).
[54] Y. Y. Lin, R. W. Chuang, S. J. Chang, S. G. Li, Z. Y. Jiao, T. K. Ko, S. J. Hon, and C. H. Liu, IEEE Photon. Technol. Lett. **24**, 1600–1602 (2012).
[55] Y. A. Yin, N. Y. Wang, G. H. Fan, and S. T. Li, IEEE Trans. Electron Devices **61**, 2849–2853 (2014).
[56] J. Piprek and Z. M. S. Li, Appl. Phys. Lett. **102**, 023510 (2013).
[57] Z.-H. Zhang, Z. Kyaw, W. Liu, Y. Ji, L. C. Wang, S. T. Tan, X. W. Sun, and H. V. Demir, Appl. Phys. Lett. **106**, 063501 (2015).
[58] J.-Y. Chang, M.-C. Tsai, and Y.-K. Kuo, Opt. Lett. **35**, 1368–1370 (2010).
[59] H. P. Zhao, G. Y. Liu, R. A. Arif, and N. Tansu, Solid-State Electron. **54**, 1119–1124 (2010).
[60] H. P. Zhao, G. Y. Liu, J. Zhang, R. A. Arif, and N. Tansu, J. Display Technol. **9**, 212–225 (2013).
[61] G. Liu, J. Zhang, C. K. Tan, and N. Tansu, IEEE Photon. J. **5**, 2201011 (2013).
[62] J.-Y. Chang and Y.-K. Kuo, Opt. Lett. **37**, 1574–1576 (2012).
[63] M. F. Schubert, J. Xu, J. K. Kim, E. F. Schubert, M. H. Kim, S. Yoon, S. M. Lee, C. Sone, T. Sakong, and Y. Park, Appl. Phys. Lett. **93**, 041102 (2008).
[64] Y. K. Kuo, T. H. Wang, J. Y. Chang, and M. C. Tsai, Appl. Phys. Lett. **99**, 091107 (2011).
[65] Y. K. Kuo, T. H. Wang, and J. Y. Chang, Appl. Phys. Lett. **100**, 031112 (2012).

[66] J. R. Chen, T. C. Lu, H. C. Kuo, K. L. Fang, K. F. Huang, C. W. Kuo, C. J. Chang, C. T. Kuo, and S. C. Wang, IEEE Photon. Technol. Lett. **22**, 860–862 (2010).
[67] N. Otsuji, K. Fujiwara, and J. K. Sheu, J. Appl. Phys. **100**, 113105 (2006).
[68] T. Li, Q. Y. Wei, A. M. Fischer, J. Y. Huang, Y. U. Huang, F. A. Ponce, J. P. Liu, Z. Lochner, J.-H. Ryou, and R. D. Dupuis, Appl. Phys. Lett. **102**, 041115 (2013).
[69] X. Ni, X. Li, J. Lee, S. Liu, V. Avrutin, Ü. Özgür, H. Morkoç, A. Matulionis, T. Paskova, G. Mulholland, and K. R. Evans, Appl. Phys. Lett. **97**, 031110 (2010).
[70] F. Zhang, X. Li, S. Hafiz, S. Okur, V. Avrutin, Ü. Özgür, H. Morkoç, and A. Matulionis, Appl. Phys. Lett. **103**, 051122 (2013).
[71] X. Li, F. Zhang, S. Okur, V. Avrutin, S. J. Liu, Ü. Özgür, H. Morkoç, S. M. Hong, S. H. Yen, T. S. Hsu, and A. Matulionis, Phys. Status Solidi A **208**, 2907–2912 (2011).
[72] X. Li, S. Okur, F. Zhang, S. A. Hafiz, V. Avrutin, Ü. Özgür, H. Morkoç, and K. Jarašiūnas, Appl. Phys. Lett. **101**, 041115 (2012).
[73] V. Avrutin, S. d. A. Hafiz, F. Zhang, Ü. Özgür, H. Morkoç, and A. Matulionis, J. Vac. Sci. Technol. A **31**, 050809 (2013).
[74] Z.-H. Zhang, W. Liu, S. T. Tan, Z. Ju, Y. Ji, Z. Kyaw, X. Zhang, N. Hasanov, B. Zhu, S. Lu, Y. Zhang, X. W. Sun, and H. V. Demir, Opt. Express **22**, A779–A789 (2014).
[75] S.-J. Chang and Y.-Y. Lin, J. Display Technol. **10**, 162–166 (2014).
[76] Z.-H. Zhang, Y. Ji, W. Liu, S. Tiam Tan, Z. Kyaw, Z. Ju, X. Zhang, N. Hasanov, S. Lu, Y. Zhang, B. Zhu, X. W. Sun, and H. V. Demir, Appl. Phys. Lett. **104**, 073511 (2014).
[77] S.-H. Yen, M.-C. Tsai, M.-L. Tsai, Y.-J. Shen, T.-C. Hsu, and Y.-K. Kuo, IEEE Photon. Technol. Lett. **21**, 975–977 (2009).
[78] Y. Ji, Z.-H. Zhang, Z. Kyaw, S. T. Tan, Z. G. Ju, X. L. Zhang, W. Liu, X. W. Sun, and H. V. Demir, Appl. Phys. Lett. **103**, 053512 (2013).
[79] S.-H. Han, D.-Y. Lee, S.-J. Lee, C.-Y. Cho, M.-K. Kwon, S. P. Lee, D. Y. Noh, D.-J. Kim, Y. C. Kim, and S.-J. Park, Appl. Phys. Lett. **94**, 231123 (2009).
[80] C. S. Xia, Z. M. S. Li, and Y. Sheng, Appl. Phys. Lett. **103**, 233505 (2013).
[81] Y. Y. Zhang and Y. A. Yin, Appl. Phys. Lett. **99**, 221103 (2011).
[82] S.-J. Lee, S.-H. Han, C.-Y. Cho, S. P. Lee, D. Y. Noh, H.-W. Shim, Y. C. Kim, and S.-J. Park, J. Phys. D, Appl. Phys. **44**, 105101 (2011).
[83] J. Kang, H. Li, Z. Li, Z. Liu, P. Ma, X. Yi, and G. Wang, Appl. Phys. Lett. **103**, 102104 (2013).
[84] J. H. Park, D. Y. Kim, S. Hwang, D. Meyaard, E. F. Schubert, Y. D. Han, J. W. Choi, J. Cho, and J. K. Kim, Appl. Phys. Lett. **103**, 061104 (2013).
[85] E. F. Schubert, W. Grieshaber, and I. D. Goepfert, Appl. Phys. Lett. **69**, 3737–3739 (1996).
[86] J. K. Kim, E. L. Waldron, Y.-L. Li, T. Gessmann, E. F. Schubert, H. W. Jang, and J.-L. Lee, Appl. Phys. Lett. **84**, 3310–3312 (2004).
[87] I. D. Goepfert, E. F. Schubert, A. Osinsky, P. E. Norris, and N. N. Faleev, J. Appl. Phys. **88**, 2030–2038 (2000).
[88] S.-J. Chang, S.-F. Yu, R.-M. Lin, S. Li, T.-H. Chiang, S.-P. Chang, and C.-H. Chen, IEEE Photon. Technol. Lett. **24**, 1737–1740 (2012).
[89] Y.-K. Kuo, J.-Y. Chang, and M.-C. Tsai, Opt. Lett. **35**, 3285–3287 (2010).
[90] B. C. Lin, K. J. Chen, C. H. Wang, C. H. Chiu, Y. P. Lan, C. C. Lin, P. T. Lee, M. H. Shih, Y. K. Kuo, and H. C. Kuo, Opt. Express **22**, 463–469 (2014).
[91] W. Yang, D. Li, N. Y. Liu, Z. Chen, L. Wang, L. Liu, L. Li, C. H. Wan, W. H. Chen, X. D. Hu, and W. M. Du, Appl. Phys. Lett. **100**, 031105 (2012).
[92] Y.-H. Lu, Y.-K. Fu, S.-J. Huang, Y.-K. Su, R. Xuan, and M. H. Pilkuhn, Appl. Phys. Lett. **102**, 143504 (2013).
[93] L. Zhang, K. Ding, N. X. Liu, T. B. Wei, X. L. Ji, P. Ma, J. C. Yan, J. X. Wang, Y. P. Zeng, and J. M. Li, Appl. Phys. Lett. **98**, 101110 (2011).
[94] L. Zhang, X. C. Wei, N. X. Liu, H. X. Lu, J. P. Zeng, J. X. Wang, Y. P. Zeng, and J. M. Li, Appl. Phys. Lett. **98**(24), 241111 (2011).
[95] J. Simon, V. Protasenko, C. Lian, H. Xing, and D. Jena, Science **327**, 60–64 (2010).
[96] C. S. Xia, Z. M. S. Li, W. Lu, Z. H. Zhang, Y. Sheng, W. D. Hu, and L. W. Cheng, J. Appl. Phys. **111**, 094503 (2012).
[97] Z. G. Ju, W. Liu, Z.-H. Zhang, T. S. Tiam, Y. Ji, Z. Kyaw, X. L. Zhang, S. P. Lu, Y. P. Zhang, B. B. Zhu, N. Hasanov, X. W. Sun, and H. V. Demir, ACS Photon. **1**, 377–381 (2014).
[98] Z.-H. Zhang, W. Liu, S. T. Tan, Y. Ji, L. Wang, B. Zhu, Y. Zhang, S. Lu, X. Zhang, N. Hasanov, X. W. Sun, and H. V. Demir, Appl. Phys. Lett. **105**, 153503 (2014).
[99] L. Zhang, K. Ding, J. C. Yan, J. X. Wang, Y. P. Zeng, T. B. Wei, Y. Y. Li, B. J. Sun, R. F. Duan, and J. M. Li, Appl. Phys. Lett. **97**, 062103 (2010).
[100] S. Li, T. Zhang, J. Wu, Y. Yang, Z. Wang, Z. Wu, Z. Chen, and Y. Jiang, Appl. Phys. Lett. **102**, 062108 (2013).
[101] S. Li, M. Ware, J. Wu, P. Minor, Z. Wang, Z. Wu, Y. Jiang, and G. J. Salamo, Appl. Phys. Lett. **101**, 122103 (2012).
[102] Z.-H. Zhang, S. T. Tan, Z. Kyaw, W. Liu, Y. Ji, Z. Ju, X. Zhang, X. W. Sun, and H. V. Demir, Appl. Phys. Lett. **103**, 263501 (2013).
[103] Y.-K. Kuo, M.-C. Tsai, S.-H. Yen, T.-C. Hsu, and Y.-J. Shen, IEEE J. Quantum Electron. **46**, 1214 (2010).
[104] Y.-K. Kuo, J.-Y. Chang, M.-C. Tsai, and S.-H. Yen, Appl. Phys. Lett. **95**, 011116 (2009).
[105] K. Zhou, M. Ikeda, J. Liu, S. Zhang, D. Li, L. Zhang, J. Cai, H. Wang, H. B. Wang, and H. Yang, Appl. Phys. Lett. **105**, 173510 (2014).
[106] C. H. Wang, S. P. Chang, W. T. Chang, J. C. Li, Y. S. Lu, Z. Y. Li, H. C. Yang, H. C. Kuo, T. C. Lu, and S. C. Wang, Appl. Phys. Lett. **97**, 181101 (2010).
[107] Y.-L. Li, Y.-R. Huang, and Y.-H. Lai, Appl. Phys. Lett. **91**, 181113 (2007).
[108] X. Ni, Q. Fan, R. Shimada, Ü. Özgür, and H. Morkoç, Appl. Phys. Lett. **93**, 171113 (2008).
[109] Z. G. Ju, W. Liu, Z.-H. Zhang, S. T. Tan, Y. Ji, Z. B. Kyaw, X. L. Zhang, S. P. Lu, Y. P. Zhang, B. B. Zhu, N. Hasanov, X. W. Sun, and H. V. Demir, Appl. Phys. Lett. **102**, 243504 (2013).
[110] J. Piprek, Appl. Phys. Lett. **104**, 051118 (2014).
[111] J. Piprek, Phys. Status Solidi RRL **8**, 424 (2014).
[112] F. Akyol, S. Krishnamoorthy, and S. Rajan, Appl. Phys. Lett. **103**, 081107 (2013).
[113] S.-J. Chang, W.-H. Lin, and C.-T. Yu, IEEE Electron Device Lett. **36**, 366 (2015).

[114] Y. Ji, Z.-H. Zhang, S. T. Tan, Z. G. Ju, Z. Kyaw, N. Hasanov, W. Liu, X. W. Sun, and H. V. Demir, Opt. Lett. **38**, 202–204 (2013).
[115] F. Zhang, N. Can, S. Hafiz, M. Monavarian, S. Das, V. Avrutin, Ü. Özgür, and H. Morkoç, Appl. Phys. Lett. **106**, 181105 (2015).
[116] S.-H. Han, C.-Y. Cho, S.-J. Lee, T.-Y. Park, T.-H. Kim, S. H. Park, S. W. Kang, J. W. Kim, Y. C. Kim, and S.-J. Park, Appl. Phys. Lett. **96**, 051113 (2010).
[117] Z.-H. Zhang, S. T. Tan, Y. Ji, W. Liu, Z. Ju, Z. Kyaw, X. W. Sun, and H. V. Demir, Opt. Express **21**, 15676–15685 (2013).
[118] C. Liu, T. Lu, L. Wu, H. Wang, Y. Yin, G. Xiao, Y. Zhou, and S. Li, IEEE Photon. Technol. Lett. **24**, 1239 (2012).
[119] Y. Li, F. Yun, X. Su, S. Liu, W. Ding, and X. Hou, J. Appl. Phys. **116**, 123101 (2014).
[120] J. P. Liu, J. B. Limb, J.-H. Ryou, D. Yoo, C. A. Horne, R. D. Dupuis, Z. H. Wu, A. M. Fischer, F. A. Ponce, A. D. Hanser, L. Liu, E. A. Preble, and K. R. Evans, Appl. Phys. Lett. **92**, 011123 (2008).
[121] A. E. Romanov, T. J. Baker, S. Nakamura, J. S. Speck, and E. J. U. Group, J. Appl. Phys. **100**, 023522 (2006).
[122] Y. Ji, W. Liu, T. Erdem, R. Chen, S. T. Tan, Z.-H. Zhang, Z. Ju, X. Zhang, H. Sun, X. W. Sun, Y. Zhao, S. P. DenBaars, S. Nakamura, and H. V. Demir, Appl. Phys. Lett. **104**, 143506 (2014).
[123] M. D. Craven, P. Waltereit, J. S. Speck, and S. P. DenBaars, Appl. Phys. Lett. **84**, 496–498 (2004).
[124] A. Chitnis, C. Chen, V. Adivarahan, M. Shatalov, E. Kuokstis, V. Mandavilli, J. Yang, and M. A. Khan, Appl. Phys. Lett. **84**, 3663–3665 (2004).
[125] A. Chakraborty, B. A. Haskell, S. Keller, J. S. Speck, S. P. DenBaars, S. Nakamura, and U. K. Mishra, Appl. Phys. Lett. **85**, 5143–5145 (2004).
[126] A. Chakraborty, B. A. Haskell, S. Keller, J. S. Speck, S. P. Denbaars, S. Nakamura, and U. K. Mishra, Jpn. J. Appl. Phys. **44**, L173 (2005).
[127] Y.-D. Lin, A. Chakraborty, S. Brinkley, H. C. Kuo, T. Melo, K. Fujito, J. S. Speck, S. P. DenBaars, and S. Nakamura, Appl. Phys. Lett. **94**, 261108 (2009).
[128] T. Detchprohm, M. Zhu, Y. Li, Y. Xia, C. Wetzel, E. A. Preble, L. Liu, T. Paskova, and D. Hanser, Appl. Phys. Lett. **92**, 241109 (2008).
[129] S.-H. Park and D. Ahn, IEEE J. Sel. Top. Quantum Electron. **19**, 1 (2013).
[130] J. Xu, M. F. Schubert, A. N. Noemaun, D. Zhu, J. K. Kim, E. F. Schubert, M. H. Kim, H. J. Chung, S. Yoon, C. Sone, and Y. Park, Appl. Phys. Lett. **94**, 011113 (2009).
[131] R. A. Arif, Y.-K. Ee, and N. Tansu, Appl. Phys. Lett. **91**, 091110 (2007).
[132] C.-T. Liao, M.-C. Tsai, B.-T. Liou, S.-H. Yen, and Y.-K. Kuo, J. Appl. Phys. **108**, 063107 (2010).
[133] R. A. Arif, H. Zhao, Y. K. Ee, and N. Tansu, IEEE J. Quantum Electron. **44**, 573 (2008).
[134] H. Zhao, G. Liu, X.-H. Li, G. S. Huang, J. D. Poplawsky, S. T. Penn, V. Dierolf, and N. Tansu, Appl. Phys. Lett. **95**, 061104 (2009).
[135] S.-H. Park, D. Ahn, and J.-W. Kim, Appl. Phys. Lett. **94**, 041109 (2009).
[136] L. T. Romano, C. G. Van de Walle, J. W. Ager, W. Götz, and R. S. Kern, J. Appl. Phys. **87**, 7745–7752 (2000).
[137] L. W. Wu, S. J. Chang, T. C. Wen, Y. K. Su, J. F. Chen, W. C. Lai, C. H. Kuo, C. H. Chen, and J. K. Sheu, IEEE J. Quantum Electron. **38**, 446 (2002).
[138] S.-N. Lee, J. Kim, K.-K. Kim, H. Kim, and H.-K. Kim, J. Appl. Phys. **108**, 102813 (2010).
[139] J.-H. Ryou, L. Jae, L. Wonseok, J. Liu, Z. Lochner, D. Yoo, and R. D. Dupuis, IEEE Photon. Technol. Lett. **20**, 1769 (2008).
[140] Z. H. Zhang, S. T. Tan, Z. Ju, W. Liu, Y. Ji, K. Zabu, D. Yilmaz, X. W. Sun, and H. V. Demir, J. Display Technol. **9**, 226 (2013).
[141] D. Y. Kim, G.-B. Lin, S. Hwang, J. H. Park, D. Meyaard, E. F. Schubert, H.-Y. Ryu, and J. K. Kim, IEEE Photon. J. **7**, 1–9 (2015).
[142] D. Han, J. Shim, D.-S. Shin, E. Nam, and H. Park, Phys. Status Solidi C **7**, 7 (2010).
[143] E. Jung, S. Kim, and H. Kim, IEEE Electron Device Lett. **34**, 277 (2013).
[144] S. Huang, B. Fan, Z. Chen, Z. Zheng, H. Luo, Z. Wu, G. Wang, and H. Jiang, J. Display Technol. **9**, 266–271 (2013).
[145] H.-Y. Ryu and J.-I. Shim, Opt. Express **19**, 2886–2894 (2011).
[146] Z.-H. Zhang, Design and Growth of High-Power Gallium Nitride Light-Emitting Diodes, PhD, School of Electrical and Electronic Engineering, Nanyang Technological University, Singapore (2014).
[147] Y. W. Cheng, H. H. Chen, M. Y. Ke, C. P. Chen, and J. J. Huang, Opt. Commun. **282**, 835–838 (2009).
[148] K. H. Lee, K. M. Kang, G. C. Hong, S. H. Kim, W. Y. Sun, and G. M. Yang, Jpn. J. Appl. Phys. **51**, 082102 (2012).
[149] J. H. Son, B. J. Kim, C. J. Ryu, Y. H. Song, H. K. Lee, J. W. Choi, and J.-L. Lee, Opt. Express **20**, A287–A292 (2012).
[150] C.-F. Tsai, Y.-K. Su, and C.-L. Lin, IEEE Photon. Technol. Lett. **21**(14), 996–998 (2009).
[151] R.-M. Lin, Y.-C. Lu, Y.-L. Chou, G.-H. Chen, Y.-H. Lin, and M.-C. Wu, Appl. Phys. Lett. **92**, 261105 (2008).
[152] T.-W. Kuo, S.-X. Lin, P.-K. Hung, K.-K. Chong, C.-I. Huang, and M.-P. Hung, Jpn J. Appl. Phys. **49**, 116504 (2010).
[153] Y.-J. Liu, C.-H. Yen, L.-Y. Chen, T.-H. Tsai, T.-Y. Tsai, and W.-C. Liu, IEEE Electron Device Lett. **30**, 1149 (2009).
[154] Y.-J. Liu, T.-Y. Tsai, C.-H. Yen, L.-Y. Chen, T.-H. Tsai, and W.-C. Liu, IEEE J. Quantum Electron. **46**, 492 (2010).
[155] Z.-H. Zhang, S. T. Tan, W. Liu, Z. Ju, K. Zheng, Z. Kyaw, Y. Ji, N. Hasanov, X. W. Sun, and H. V. Demir, Opt. Express **21**, 4958–4969 (2013).
[156] Z. Kyaw, Z.-H. Zhang, W. Liu, S. T. Tan, Z. G. Ju, X. L. Zhang, Y. Ji, N. Hasanov, B. Zhu, S. Lu, Y. Zhang, X. W. Sun, and H. V. Demir, Opt. Express **22**, 809–816 (2014).
[157] S. R. Jeon, M. S. Cho, M.-A Yu, and G. M. Yang, IEEE J. Sel. Top. Quantum Electron. **8**, 739 (2002).
[158] S. R. Jeon, Y. H. Song, H. J. Jang, K. S. Kim, G. M. Yang, S. W. Hwang, and S. J. Son, Phys. Status Solidi A **188**, 167 (2001).
[159] S.-R. Jeon, Y.-H. Song, H.-J. Jang, G. M. Yang, S. W. Hwang, and S. J. Son, Appl. Phys. Lett. **78**, 3265–3267 (2001).

[160] T. Tetsuya, H. Ghulam, C. Scott, H. Mark, R. P. Schneider, Jr., K. Chris, B. Mats, Y.-I. Chang, L. Dale, R. K. Mike, W. C. Lou, and A. S. Steve, Jpn. J. Appl. Phys. **40**, L861 (2001).
[161] C.-M. Lee, C.-C. Chuo, I. L. Chen, J.-C. Chang, and J.-I. Chyi, IEEE Electron Device Lett. **24**, 156 (2003).
[162] Z.-H. Zhang, S. T. Tan, Z. Kyaw, Y. Ji, W. Liu, Z. Ju, N. Hasanov, X. W. Sun, and H. V. Demir, Appl. Phys. Lett. **102**, 193508 (2013).
[163] S. Krishnamoorthy, F. Akyol, P. S. Park, and S. Rajan, Appl. Phys. Lett. **102**, 113503 (2013).
[164] Y. P. Zhang, Z.-H. Zhang, W. Liu, S. T. Tan, Z. G. Ju, X. L. Zhang, Y. Ji, L. C. Wang, Z. Kyaw, N. Hasanov, B. B. Zhu, S. P. Lu, X. W. Sun, and H. V. Demir, Opt. Express **23**, A34–A42 (2015).
[165] A. Hangleiter, F. Hitzel, C. Netzel, D. Fuhrmann, U. Rossow, G. Ade, and P. Hinze, Phys. Rev. Lett. **95**, 127402 (2005).
[166] Y.-H. Cho, J.-Y. Kim, J. Kim, M.-B. Shim, S. Hwang, S.-H. Park, Y.-S. Park, and S. Kim, Appl. Phys. Lett. **103**, 261101 (2013).
[167] J. Kim, Y.-H. Cho, D.-S. Ko, X.-S. Li, J.-Y. Won, E. Lee, S.-H. Park, J.-Y. Kim, and S. Kim, Opt. Express **22**, A857–A866 (2014).
[168] S.-H. Han, D.-Y. Lee, H.-W. Shim, J. Wook Lee, D.-J. Kim, S. Yoon, Y. S. Kim, and S.-T. Kim, Appl. Phys. Lett. **102**, 251123 (2013).
[169] K. Koike, S. Lee, S. R. Cho, J. Park, H. Lee, J.-S. Ha, S.-K. Hong, L. H.-Y. Lee, M.-W. Cho, and T. Yao, IEEE Photon. Technol. Lett. **24**, 449 (2012).
[170] L. C. Le, D. G. Zhao, D. S. Jiang, L. Li, L. L. Wu, P. Chen, Z. S. Liu, J. Yang, X. J. Li, X. G. He, J. J. Zhu, H. Wang, S. M. Zhang, and H. Yang, J. Appl. Phys. **114**, 143706 (2013).
[171] J. Kim, Y. Tak, J. Kim, S. Chae, J.-Y. Kim, and Y. Park, J. Appl. Phys. **114**, 013101 (2013).
[172] L. C. Le, D. G. Zhao, D. S. Jiang, L. Li, L. L. Wu, P. Chen, Z. S. Liu, Z. C. Li, Y. M. Fan, J. J. Zhu, H. Wang, S. M. Zhang, and H. Yang, Appl. Phys. Lett. **101**, 252110 (2012).
[173] Y. Li, S. You, M. Zhu, L. Zhao, W. Hou, T. Detchprohm, Y. Taniguchi, N. Tamura, S. Tanaka, and C. Wetzel, Appl. Phys. Lett. **98**, 151102–151103 (2011).
[174] J.-Y. Chang, F.-M. Chen, Y.-K. Kuo, Y.-H. Shih, J.-K. Sheu, W.-C. Lai, and H. Liu, Opt. Lett. **38**, 3158–3161 (2013).
[175] R. Vaxenburg, A. Rodina, E. Lifshitz, and A. L. Efros, Appl. Phys. Lett. **103**, 221111 (2013).
[176] Z.-H. Zhang, W. Liu, Z. Ju, S. T. Tan, Y. Ji, Z. Kyaw, X. Zhang, L. Wang, X. W. Sun, and H. V. Demir, Appl. Phys. Lett. **105**, 033506 (2014).
[177] H. Hirayama, Proc. SPIE **7987**, 79870G (2011).
[178] A. Khan, K. Balakrishnan, and T. Katona, Nature Photon. **2**, 77 (2008).

